Acta Pharmaceutica Sinica B 2024;14(7):3009−3026

Chinese Pharmaceutical Association
Institute of Materia Medica, Chinese Academy of Medical Sciences

Acta Pharmaceutica Sinica B

www.elsevier.com/locate/apsb
www.sciencedirect.com

ORIGINAL ARTICLE

Exosomes derived from tumor adjacent fibroblasts efficiently target pancreatic tumors

Saini Setua[a], Shabia Shabir[b], Poornima Shaji[c,d], Ana Martinez Bulnes[c,d], Anupam Dhasmana[c,d,e], Swathi Holla[c], Nivesh K. Mittal[f], Nirakar Sahoo[g], Tripti Saini[g], Francesco Giorgianni[a], Mohammad Sikander[a,c,d], Andrew E. Massey[a,h], Bilal B. Hafeez[a,c,d], Manish K. Tripathi[a,c,d], Vincent P. Diego[i], Meena Jaggi[a,c,d], Junming Yue[a], Nadeem Zafar[j], Murali M. Yallapu[a,c,d], Stephen W. Behrman[a,k,l,*], Sheema Khan[a,c,d,*], Subhash C. Chauhan[a,c,d,*]

[a]*Department of Pharmaceutical Sciences, College of Pharmacy, and College of Medicine, University of Tennessee Health Science Center (UTHSC), Memphis, TN 36163, USA*
[b]*Department of Computer Science, Islamic University of Science and Technology, Awantipora, J&K 192122, India*
[c]*Department of Immunology and Microbiology, School of Medicine, University of Texas Rio Grande Valley, McAllen, TX 78504, USA*
[d]*South Texas Center of Excellence in Cancer Research, School of Medicine, the University of Texas Rio Grande Valley, McAllen, TX 78504, USA*
[e]*Himalayan School of Biosciences and Cancer Research Institute, Himalayan Institute of Medical Sciences, Swami Rama Himalayan University, Dehradun 248016, India*
[f]*Plough Center for Sterile Drug Delivery Solutions, UTHSC, Memphis, TN 38104, USA*
[g]*Department of Biology, College of Sciences, UTRGV, McAllen, TX 78539, USA*
[h]*National Institute of Biomedical Imaging and Bioengineering (NIBIB), National Institutes of Health, Bethesda, MD 20892, USA*
[i]*South Texas Diabetes and Obesity Institute, UTRGV, McAllen, TX 78504, USA*
[j]*Dept. of Laboratory Medicine & Pathology, University of Washington, Seattle, WA 98195, USA*
[k]*Department of Surgery, Baptist Memorial Medical Education, Baptist Memorial Hospital, Memphis, TN 38120, USA*
[l]*Baptist Health Sciences University, Memphis, TN 38104, USA*

Received 26 September 2023; received in revised form 25 January 2024; accepted 26 January 2024

*Corresponding authors.
E-mail addresses: stephen.behrman@baptistu.edu (Stephen W. Behrman), sheema.khan@utrgv.edu (Sheema Khan), subhash.chauhan@utrgv.edu (Subhash C. Chauhan).

Peer review under the responsibility of Chinese Pharmaceutical Association and Institute of Materia Medica, Chinese Academy of Medical Sciences.

https://doi.org/10.1016/j.apsb.2024.04.003

KEY WORDS

Pancreatic cancer;
Tumor adjacent normal tissue fibroblasts (NAF);
Desmoplasia;
Extracellular vesicles;
Exosomes;
Tumor targeting;
Ormeloxifene;
Personalized medicine

Abstract The application of extracellular vesicles, particularly exosomes (EXs), is rapidly expanding in the field of medicine, owing to their remarkable properties as natural carriers of biological cargo. This study investigates utilization of exosomes derived from stromal cells of tumor adjacent normal tissues (NAF-EXs) for personalized medicine, which can be derived at the time of diagnosis by endoscopic ultrasound. Herein, we show that exosomes (EXs) derived from NAFs demonstrate differential bio-physical characteristics, efficient cellular internalization, drug loading efficiency, pancreatic tumor targeting and delivery of payloads. NAF-derived EXs (NAF-EXs) were used for loading ormeloxifene (ORM), a potent anti-cancer and desmoplasia inhibitor as a model drug. We found that ORM maintains normal fibroblast cell phenotype and renders them incompatible to be triggered for a CAF-like phenotype, which may be due to regulation of Ca^{2+} influx in fibroblast cells. NAF-EXs-ORM effectively blocked oncogenic signaling pathways involved in desmoplasia and epithelial mesenchymal transition (EMT) and repressed tumor growth in xenograft mouse model. In conclusion, our data suggests preferential tropism of NAF-EXs for PDAC tumors, thus imply feasibility of developing a novel personalized medicine for PDAC patients using autologous NAF-EXs for improved therapeutic outcome of anti-cancer drugs. Additionally, it provides the opportunity of utilizing this biological scaffold for effective therapeutics in combination with standard therapeutic regimen.

1. Introduction

Pancreatic ductal adenocarcinoma (PDAC) is an extremely lethal form of cancer characterized by its intricate tumor histoarchitecture and challenges in diagnosis and treatment, primarily due to limited drug accumulation at the tumor site. Consequently, within a span of two years, tumor relapse commonly occurs, either as local recurrence or widespread metastasis[1]. The detection of tumor relapse through imaging becomes challenging due to the extensive postoperative changes in the surrounding region following tumor resection. Notably, metastatic recurrence rates surpass those of local recurrence[1]. This phenomenon is attributed to the resilient and inflexible nature of tumors, which enable them to regrow even from a single remaining tumor cell. Recurrent PDAC displays a higher level of adaptability compared to the primary disease, exhibiting distinct genomic characteristics, intermetastatic genetic heterogeneity, diverse clonal origins, and a higher mutational burden than observed in the primary cancer[2]. Consequently, effective management necessitates a treatment approach that outsmarts the tumor and can manipulate the intricate tumor microenvironment to impede its spread.

The effectiveness of a therapeutic drug in treating tumors and tumor cells relies on its ability to accumulate adequately within them. In the case of PDAC, the presence of a dense fibrotic tumor microenvironment, along with an excessive amount of stroma, hinders treatments from reaching the tumors in the necessary dosage levels. The abundance of tumor stroma and the limited presence of blood vessels can partially explain why delivering therapeutic concentrations of drugs has proven challenging in achieving effective treatments for PDAC. One promising approach involves identifying specific tumor characteristics and developing personalized therapeutic options, which holds the potential to provide more effective management of PDAC.

Recently, exosomes (EXs) have gained a lot of interest in the scientific field. These are extracellular vesicles (EVs)[3], which are in the size range of 30−150 nm[4] and can deliver therapeutic cargo(s) into the target cells[5]. It is shown that EXs have cell membranes[6] and can protect their cargo from degradation being stable in systemic circulation, thus are attractive tool for diagnostic and therapeutic applications[4]. However, the utilization of EXs requires a customization based on information about individual patients and responses to specific treatment[4]. In order to avoid the non specific consequences of the same, utilizing an autologous exosomes seems to be an excellent option that can be applied as a personalized medicine to match the individual circumstances and molecular profile of the patient. Due to their similarity to one's own cellular system, these exosomes have the potential to evade recognition as foreign entities. Research indicates that autologous exosomes, which are derived from the individual's own cells, possess immune privilege and safety advantages, effectively avoiding immunological reactions often linked to foreign exosomes[7]. The emergence of autologous-origin exosomes is attributed to their demonstrated safety and efficacy in mouse models[8] and clinical trials[9]. The non-immunogenic characteristics of exosomes make them particularly appealing as a means of delivering drugs, especially when isolated from the individual's own body, thereby making them an enticing component for personalized medicine. The main goal of current investigation is to develop a newer strategy to improve drug accumulation at tumor bed using EXs obtained from the fibroblasts isolated from normal appearing tumor adjacent tissues.

Therefore, the current study demonstrates an optimized exosome-based stroma targeting therapeutic intervention using autologous EXs derived from fibroblast cells that are isolated from patient's matched adjacent normal tissue (NAF) surrounding pancreatic tumor tissue for treatment of pancreatic cancer. Our study demonstrates that these EXs can efficiently target and accumulate in pancreatic tumors. Since these EXs are inherently equipped to deliver cargos in the tumors as a natural phenomenon to restrict tumor growth, our strategy presents natural vehicles for the tumor targeted delivery of cancer therapeutics into the tumor microenvironment, interrupting the signals erupting thereof and thereby preventing the formation of a pre-metastatic niche. The proposed concept can be highly useful for the patients that are eligible for surgical resection. We have utilized this EXs based scaffold for delivery of a drug, ormeloxifene (ORM), that we

recently identified as a tumor stroma modulator and potent anti-cancer agent[10]. Our results highlight the prospects of using this methodology to enhance accessibility of therapeutic payload in pancreatic tumors with low or no immunogenic responses.

2. Materials and methods

2.1. Human cell culture

Pancreatic cancer cell lines, HPAF-II, AsPC-1 and Panc-1 were purchased from ATCC (American Type Cell Culture) and cultured using Dulbecco's modified Eagle's medium (DMEM)-F12/DMEM medium (HyClone Laboratories, Inc.), which was supplemented with 10% FBS (fetal bovine serum; Gibco) and antibiotic/antimycotic solution at 37 °C in a humidified atmosphere (5% CO_2 and 95% air atmosphere). A new vial (from a stock of frozen vials) was used every 6 months to maintain validity of the cell lines used for the experimentation. Mycoplasma testing in cells is routinely performed. Deidentified, pancreatic tumor and matched adjacent normal waste tissues were collected at Baptist Memorial Hospital, Memphis after appropriate IRB approval. Cancer associated fibroblasts (CAF) and matched adjacent normal fibroblasts (NAF) were isolated from the respective tissues by outgrowth method for secretion of EXs[11] (Fig. 1A). Briefly, pancreatic cancer and matched adjacent normal tissue waste were seeded in separate 100 mm dishes in the form of small tissue (0.5−1 mm^3) blocks in the presence of 10%−20% FBS and DMEM growth medium supplemented with L-glutamine (2 mmol/L), antibiotic and antimycotic solutions. Tissue blocks were cultured at 37 °C in a 5% CO_2-air humidified atmosphere and monitored for outgrowth of cells for 2−4 days. Fibroblast cell population was enriched through the brief trypsinization process and characterized by cytofilament staining (α-SMA/Hyaluronic acid/Desmin). EXs were isolated from NAF and CAF using Total Exosome Isolation Reagent while culturing them in exosome depleted FBS media (Exo-FBS™ Exosome-depleted FBS media, SBI System Biosciences). Cell free conditioned media was processed for exosomes isolation according to manufacturer instructions by centrifugation method using Total Exosome Isolation Reagent (Thermo fisher scientific). The obtained pellet of extracellular vesicles was suspended in PBS and following measuring protein concentration using Bradford method. The exosome suspension was stored at −80 °C until further use.

2.2. Proteomic analysis of EXs and pathway enrichment of genes interaction network

Extracellular vesicles (EXs) isolated from CAF and NAF were processed for proteomic sample preparation for mass spectrometry analysis (using IST 8X from Preomics). Proteomics was

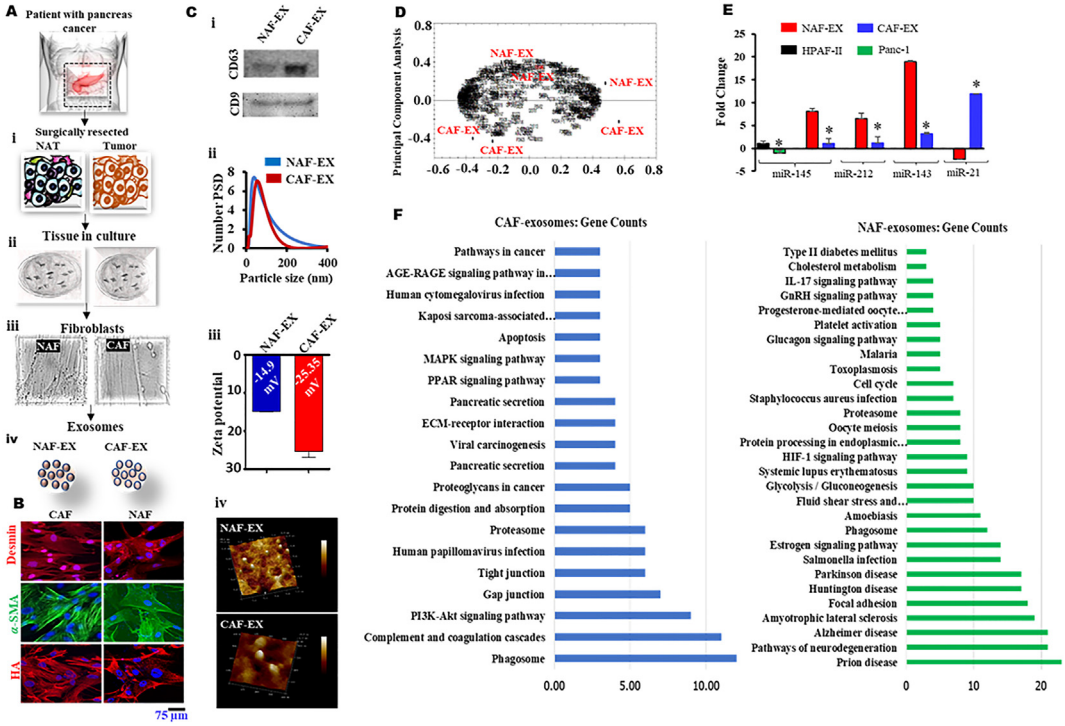

Figure 1 Bio-physical characterization of EXs from pancreatic tissue fibroblasts. (A) Graphical representation of isolation of matched adjacent normal tissue and tumor tissues (i) followed by culture of fibroblast cells (ii, iii) and EXs isolation (iv). Data represents mean ± SEM; $n = 3$. (B) Isolated NAF and CAF were assessed by cytofilament staining (Desmin, α-SMA and hyaluronic acid (HA)) using immunofluorescence assay. (Ci) Immunoblotting of exosome marker proteins CD63 and CD9 expression for both NAF-EX and CAF-EX derived EXs. An equal amount of protein was used for the assay. (Cii) Graph representing number percentage *versus* particle size of NAF-EX and CAF-EX. (Ciii) Graph demonstrates zeta potential of NAF-EX and CAF-EX. (Civ) Shape and surface morphology of NAF and CAFs derived EXs were identified by AFM image. (D) Software-based principal component analysis of 3 NAF-EX and 3 CAF-EX samples. (E) Tumor suppressor microRNAs (miR-145/143/212) and oncogenic miRNA (miR-21) fold expression in NAF and CAFs. Data represents mean ± SEM, $n = 3$; $^*P < 0.005$. (F) Pathway enrichment analysis of genes selected from CAF (left) and NAF (right) EXs.

performed using LC−MS and analyzed using discovery analysis software, progenesis QI. The proteomic data was used to identify differentially expressed genes among NAF and CAF. The details of altered input genes (230 normal genes & 182 cancer genes) were obtained from the EXs of NAF and CAF. The selection criteria of normal and cancer genes among all the genes present in EXs was based on highest mean condition from raw data (Supporting Information Tables S1 and S2)[12]. These lists of genes were used for the construction of gene interaction network (GIN) by using GeneMANIA on the bases of genetic interactions, co-expression, co-localization, pathway, physical interactions, predicted interaction and shared protein domains. The GIN input file was imported in the cytoscape for the pathways enrichment analyses by using KEGG plugin. The cytoscape was used for the construction of the final GIN of both normal and cancer genes separately. Due to better size, charge and tumor protecting features, we utilized NAF derived EXs for further experimentation.

2.3. EXs mediated RNA and protein uptake assay

To monitor cellular uptake and cancer cell targeting potential, EXs were labelled with Exo-Glow as per manufacturer instructions. Briefly, EXs were isolated from the NAF and CAF cells grown to 70%−80% confluence in exosome-depleted media. The EXs suspension (500 μL) containing 1 μg/μL) was labeled with 50 μL of 10x Exo-Red or Exo-Green for 10 min at 37 °C. Labeled EXs were separated using ExoQuick-TC kit.

2.4. Characterization of drug loaded EXs

NAF derived EXs were used for generating formulation with ormeloxifene drug (NAF-EX-ORM). ORM was synthesized by Prof. Fathi Halaweish from University of South Dakota by following a standardized protocol described in our earlier publication[13]. We have described its synthesis earlier in our publication. ORM solution (1 mg/mL) was mixed with the EXs at room temperature for ∼30 min at different concentration of EXs (protein 100, 400 and 500 μg). To remove the free drug, EXs solution was centrifuged at 10,000 rpm (Centrifuge 5920 R, Eppendorf) for 10 min and then washed twice with PBS and was stored at −80 °C. After dilution in PBS and particle size and poly dispersity index (PDI) of NAF-EX-ORM formulation were analyzed using a Zetasizer (Malvern Instruments Ltd., Malvern, Worcestershire, UK). Drug loading efficiency of the different NAF-EX-ORM formulations was determined by UPLC analysis. Briefly, 0.9 mL acetonitrile was added to 100 μL of NAF-EX-ORM formulation to extract the drug and precipitate EXs proteins. The precipitated proteins were separated by centrifugation at 10,000×*g* for 10 min. Supernatant containing drug was analyzed the Waters® H-Class UPLC to determine the ORM concentration. For this assay, we used CORTECS® T3 1.6 μm column, solvent A (0.1% formic acid), solvent B (acetonitrile with 0.1% formic acid) with a 2-min gradient elution (minutes/%A 0/90, 0−1/10, 1−1.10/90, 1.10−2/90). UV λ_{max} at 220 nm was used for detection using a PDA detector and the retention time for ORM using the above conditions was 1.0 ± 0.1 min. Finally, for all experiments detailed in this article, we calculate the treatment volume of the formulation based on the ORM loading concentration equivalent of the final desired ORM concentration of 20 μmol/L for *in vitro* and 200 μg per mouse for *in vivo* studies, as standardized in our earlier publication[10].

2.5. Atomic force microscopy

Topological differences among NAF and CAF derived EXs were determined by atomic force microscopy (AFM). For Atomic force microscopy (AFM), EVs samples were placed on a silica wafer and air dried for 30 min for AFM imaging in tapping mode using aluminum-coated silicon probes. Topographic height, amplitude and phase retraces were imaged concurrently with a fixed force (<1 nN) with a scanning rate of 1 Hz. The images were recorded at 256 × 256 pixels and processed using IGOR software.

2.6. Trafficking and subcellular localization of EXs

To determine the trafficking and subcellular localization of NAF EXs, pancreatic cancer cells (8×10^4) were seeded on 4-well chamber glass slides, treated with EXs (15 μg) and grown for 24 h. Cells were then fixed (using 4% paraformaldehyde), permeabilized (0.1% TritonX-100), and washed with PBS, followed by a blocking step (10% donkey serum in PBS). After that, cells were incubated with Mito Tracker Red (30 nmol/L) or LysoTrackerR Red (75 nmol/L) DND-99 (Life Technologies) to stain mitochondria and lysosome, respectively. Internalization and subcellular localization of EXs was confirmed by CD63 expression and DAPI (4′,6-diamidino-2-phenylindole, Life Technologies) was for nuclear stating. Finally, slides were mounted in Vectashield Mounting Medium (Vector Labs, Burlingame, CA, USA) before visualization under the confocal microscope (Carl Zeiss LSM 710, Oberkochen, Germany) at different magnifications.

2.7. Functional tumorigenic assays

To determine the *in-vitro* therapeutic efficacy of the NAF-EX-ORM formulation, cell proliferation (MTT assay), real time xCELLigence, cellular migration (Boyden chamber) and invasion (Matrigel invasion chambers) assay were performed as described earlier[10]. Cell proliferation assays were performed using standard MTT 3-(4,5-dimethyl-2-thiazolyl)-2,5-diphenyl-2*H*-tetrazolium-bromide) with PanCa cell lines (HPAF-II, and AsPC-1). Briefly, cells were seeded at 5000 cells/well in 96-well plates and treated with various concentration of free ORM (20 μmol/L) and NAF-EX-ORM (equivalent to 20 μmol/L) in presence or absence of EGF for 48 h and then MTT reagent was added. The absorbance was measured at 570 nm using BioTek™ Cytation™ 3 and the percentage of cell proliferation was determined among control and experimental treated groups. Cell migration assay was performed using Boyden's chamber method. For that, 6−8 h serum starved cells (50,000 cells/well) were plated at in upper chambers and then treated with blank EXs or free ORM (20 μmol/L) and NAF-EX-ORM (equivalent to 20 μmol/L) formulation in presence or absence of EGF for 10−12 h. Cells that migrated towards lower chamber were fixed with 4% paraformaldehyde and stained with crystal violet. Cells remaining in the upper chamber were removed by cotton swab and then migrated cells were observed/imaged by using light microscope. For invasion assay, similar protocol and treatments were used using Matrigel coated 24 Transwell Boyden chamber in serum free culture medium. To further confirm the effect of NAF-EX-ORM formulation on these tumorigenic features, we performed real-time cell proliferation, migration and invasion assays using RTCA xCELLigence platform. xCELLigence system is a microelectronic biosensor cell-based assay.

Based on cellular viability, number, morphology and adhesion characteristics, this instrument provides electrical impedance which represents a real time behavior of cells. We performed cell proliferation, migration, and invasion using xCELLigence System as described in our previous publications. Briefly, cells were seeded in respective plates for cell proliferation, migration, invasion and treated with free ORM (20 μmol/L) and NAF-EX-ORM (equivalent to 20 μmol/L) and results were analyzed through xCELLigence instrument.

2.8. Cell cycle analysis and apoptosis

Cell cycle analysis was performed to determine the effect of NAF-EX-ORM on cell cycle as described earlier[10]. Briefly, cells (2×10^6) were plated in 100-mm dish, allowed to adhere overnight and then treated with different formulations [EXs, free ORM (20 μmol/L) and NAF-EX-ORM (equivalent to 20 μmol/L)] for 24 h. After that, cells were trypsinized, washed, fixed (70% ice cold EtOH) and saved at −20 °C until further used. At the time of analysis, cells will be incubated with RNase at 37 °C for 90 min and stained with Propidium Iodide (PI) solution (Sigma−Aldrich, St. Louis, MO, USA) for 30 min and analyzed by Accuri C6 flow cytometer in FL2 channel. Data interpretation was performed by ModFit.Lt software. Induction of apoptosis was measured by utilizing Annexin V PE kit. For that, cells were plated (1×10^6/plate) and treated with above mentioned treatment groups. After 24 h, both floaters and adherent cells were collected, washed and stained with Annexin V (5 μL/100 μL of cell suspension concentration) for 20 min in the dark and then were analyzed with Accuri C6 flow cytometer in FL2 channel. Data was represented with early and late apoptotic population with graphical representation.

2.9. Western blotting

Western blotting analysis was performed to determine molecular effect of different treatment groups on [ORM, free ORM (20 μmol/L) and NAF-EX-ORM (equivalent to 20 μmol/L)] using human PanCa cells (HPAF-II and AsPC1) and the expression of several key proteins associated with EMT and SHH signaling pathway was evaluated as described earlier[10]. Immunoblotting analysis was also performed using tumor tissue proteins extracts that were prepared by homogenizing in Tissue Extraction reagent-1 (Life Technologies) as described earlier.

2.10. Quantitative real-time PCR (qRT-PCR)

Total RNA was extracted from the treated and untreated cells (HPAF-II and AsPC-1) using TRIzol reagent and the concentration of RNA was quantified by Nanodrop instrument 2000 (Thermo Scientific). The expression level of mRNA was evaluated by qRT-PCR using specific set of primers. GAPDH was used as an endogenous housekeeping control as previously explained protocol.

2.11. Immunofluorescence (cells and tissue)

Immunofluorescence analysis was carried out in PanCa cells and excised tumor tissues as per previously described protocol[10]. This assay was performed to determine the expression and subcellular localization of key proteins that are related to desmoplasia and EMT pathways. Tumor tissues sections were deparaffinized, rehydrated followed by heat induced antigen retrieval to stain for specific antibodies (α-SMA, collagen, vimentin and E-cadherin).

2.12. Spheroid assay

Tumor spheroid assay was performed as described earlier[10]. We have investigated the effect of EXs, free ORM (20 μmol/L) and NAF-EX-ORM (equivalent to 20 μmol/L) as compared to control on spheroid formation and growth which imitate the tumor like situation under *in vitro* conditions. HPAF-II and AsPC-1 cells (1000/well) were seeded in 96-well low attachment plate (Corning) in 0.5% serum free medium and allowed them to form small primary spheroids (for 3−5 days) followed by above mentioned treatments. Following one-week incubation, primary spheroids were dissociated into single cells and plated into 6 well low attachment plates at a density of 1×10^4 per well and allowed them to grow another 10 days without adding any treatment. The size of spheroids was measured, graphed and photographs were taken to determine therapeutic efficacy of each treatment group.

2.13. Live cells Ca^{2+} imaging

Live cell Ca^{2+} imaging was performed as previously described earlier[14] with our modified protocol described in Supporting Information section. Briefly, ASPC1 cells were cultured to 70%−80% confluence on polylysine-coated glass coverslips and then spiked with 100 nmol/L EGF before ORM (20 μmol/L) treatment for 24 h. Following treatment, the cells were loaded with Fluo-4/AM (4 μmol/L) (Invitrogen Molecular Probes, Eugene, OR, USA) along with PowerLoad concentrate 100 × (Invitrogen Molecular Probes, Eugene, OR, USA) for 1 h at 37 °C. The stained live-cells were imaged through Olympus IX 71 inverted microscope that is attached with PTI easy-ratio pro system (PTI, HORIBA Scientific, North Edison, NJ, USA) and pco. Panda SCMOS camera. Ca^{2+} release was measured in Tyrode's solution at an excitation wavelength of 488 nm. Ionomycin (6.7 mmol/L) (AlfaAesar, Haverhill, MA, USA) and BAPTA-AM (26 mmol/L) (1,2-bis(*o*-aminophenoxy) ethane-*N,N,N′,N′*-tetraacetic acid; Invitrogen Molecular Probes™ Eugene, OR, USA)), 2 μL were dropped into the Tyrode's solution during the live measurements to measure the change in the Fluo-4 fluorescence intensity. The relative basal Ca^{2+} signal in control (untreated), EGF, and ormeloxifene treated cells was calculated by dividing the basal fluorescence intensity by the ionomycin-induced maximum fluorescence intensity of the same cell. Ionomycin, a Ca^{2+} ionophore, was added to the cells to induce a maximum Ca^{2+} signal and was normalized to 1. The BAPTA-AM, a potent Ca^{2+} chelator was added to the cells to test if the Flou-4-AM fluorescence intensity is associated with intracellular Ca^{2+} ions. Ca^{2+} imaging data were analyzed using EasyRatioPro (PTI, HORIBA Scientific, North Edison, NJ, USA) software and later processed with Excel (Microsoft, Redmond, WA, USA) and Igor Pro v8.0 (Wavemetrics, Lake Oswego, OR, USA) software. Figures were created using Origin Pro v2020 (Originlab, Northampton, MA, USA) and ImageJ (NIH).

2.14. In vivo xenograft mice model

Six weeks-old *nu/nu* mice were purchased from Jackson laboratories and maintained in a pathogen-free environment with all procedures approved by the UTHSC Institutional Animal Care and Use Committee (IACUC). HPAF-II luciferase cells (3×10^6) and a mixture of human pancreatic stromal cells (1.5×10^6) were

suspended in 1:1 PBS and Matrigel (BD Biosciences) solution and injected subcutaneously in the right flank of each mouse as described earlier[15]. Mice were treated intraperitoneally with EX and NAF-EX-ORM (equivalent to 200 μg)[10] twice a week for five weeks. Finally, the tumor volume (V) was evaluated using length (L), width (W), and height (H) and calculated by Eq. (1):

$$\text{Volume } (\text{mm}^3) = 0.5 \times L \times W \times H \quad (1)$$

Mice were sacrificed as soon as tumor volume reached to 1000 mm^3, and tumors, other organs were harvested for *ex vivo* imaging. Some portions of tissues were used for the preparation of whole lysate for immunoblotting, RNA isolation and remaining tissues were fixed with 10% formalin for paraffin embedding, and histochemical analyses.

2.15. Immunohistochemistry

Immunohistochemistry (IHC) was performed on 5 μm thick tissue sections for protein expression analysis as described earlier[16]. Tissue sections were deparaffinized, rehydrated followed by heat induced antigen retrieval and then processed for IHC using specific antibodies such as, N-cadherin, β-catenin, hyaluronic acid, and Ki67.

2.16. Statistical analysis

Statistical analyses were performed using Student's t test, GraphPad Prism software when comparing two variables or two-way ANOVA when comparing more than two variables. Data are expressed as mean ± standard error (SE) values. Calculated differences as $^{*}P < 0.05$, $^{**}P < 0.01$, and $^{***}P < 0.001$ were considered significant.

3. Results

3.1. EXs released by NAF and CAF are bio-physically distinct

Extracellular vesicles (EXs) offer a therapeutic avenue towards personalized medicine[17]. Toward this effort, we have bio-physically characterized EXs that are released by the normal adjacent tissue fibroblast (NAFs) and cancer tissue associated fibroblast (CAFs). Our bio-physical characterization analyses suggest considerable differences in size, charge, and cargoes of EXs that are released from NAFs as compared to CAFs. Both CAF and NAF have demonstrated the expression of stromal cell markers such as Desmin, α-SMA, and Hyaluronic acid (HA) (Fig. 1B). EXs released from NAFs were evaluated for the expression of CD63 and CD9 (EXs markers) using immunoblotting. Both EXs demonstrated the expression of CD63 and CD9, which confirms purity of the EXs (Fig. 1Ci). These EXs were relatively smaller with lesser negative zeta potential (∼44.12 ± 0.89 nm with −14.9 mV) as compared to CAFs (70.28 ± 1.47 nm with −25.3 mV) (Fig. 1Cii and iii, Fig. 2 Inset table 2). Our AFM analysis suggested perfect round shape morphology of these EXs NAF and CAFs and confirmed the size range that was identified by DLS. The results depicted high-resolution topography of the CAFs and NAFs EXs, which is identified by interactions between the sample and the nanoindentation probe (Fig. 1Civ). Mass spectrometry is a prominent strategy for comprehensive analysis of proteins in complex biological systems. We evaluated the proteomic profile of NAFs and CAFs released EXs using a typical proteomic bioanalytical workflow. We analyzed a total of 3 NAFs and 3 CAFs EXs samples. The NAFs were generated through matched normal adjacent tissue (NAT), the area that is surrounding the tumor tissue and is histologically normal and collected according to TCGA protocols (>2 cm from the tumor margin and/or does not contain tumor by histopathologic review)[18,19]. This is the area that is inherently adopted for early defensive mechanisms against the tumor. This defense mechanism of NAT is expected to be orchestrated by the tumor suppressive EXs cargo which motivated us to perform comparative proteomic analysis of NAFs and CAFs EXs. Interestingly, our results demonstrate distinct molecular cargo signatures in EXs obtained from NAFs as compared to CAF-EXs. This molecular level difference is represented by a histogram of 100,000 simulations in R for the subspace distance among the NAFs *versus* CAFs EXs (Supporting Information Fig. S1). These differences are also well captured in Principal component analysis (Fig. 1D), which was capable of distinguishing nicely the cancer derived samples from the normal derived ones. Additionally, we were interested to investigate the expression of microRNAs, since they form important cargo in EXs that are essentially transported to neighboring cells/tissues[20]. We particularly focused on miRNAs that have shown association with pancreatic cancer such as, tumor suppressor microRNAs (miR-145, miR-143 and miR-212) and oncogenic miRNA (miR-21). Our results showed that the NAFs EXs expressed substantially higher quantities of tumor suppressor miRs (miR-145; ∼10 folds, miR-143; ∼7 folds and miR-212; ∼20 folds) as compared with CAF-EXs (Fig. 1E and Supporting Information Fig. S2A). In contrary CAFs EXs exhibited very high expression of oncogenic miRs (miR-21; ∼12 folds), while NAFs EXs have shown almost no expression of this oncogenic miR. With these striking observations in NAF EXs, we sought to check these patterns in fibroblast cells, NAF and CAF. We particularly investigated miR-145, being a universal tumor suppressor, in both NAF and CAF and found similar results showing greater fold expression in NAF than CAF (Fig. S2B). This indicates that NAF-EXs carry higher amount of tumor suppressor molecular cargoes as compared to CAFs EXs.

To further elaborate this molecular signature study, we performed GIN and pathways enrichment analyses of these EXs. In this study, we have identified that the input proteins from the CAFs EXs are carrying molecular cargoes that are associated with oncogenic pathways like, MAPK signaling, PPAR signaling, Viral carcinogenesis, Proteoglycans, and PI3K−Akt signaling pathway (Fig. 1F, Supporting Information Fig. S3). Our study demonstrates around 20 enriched pathways, which have a direct and/or indirect association with cancer progression. While genes identified in the NAFs EXs have shown the abundant expression of genes/pathways that are relevant to tumor suppressive and/or apoptosis functions (Fig. 1F, Supporting Information Fig. S4). Collectively, these results demonstrate the presence of distinct molecular cargos in EXs isolated from NAFs and CAFs (Tables S1 and S2). These results explain how NAT tissue provide protective mechanisms to tumor spread[19]. Based on these observations, we selected NAFs-EXs to investigate if these biological vehicle/autologous tool can be useful for the tumor targeted delivery of cancer therapeutics in pancreatic cancer model.

Additionally, we employed machine learning-based method for automatic resolution of the whole mass spectrometry data to extract the meaningful features swamped by the noises. We utilized a method of feature selection that filters out critical (strong) features (proteins) contributing towards the efficient predictive modeling. This is done to

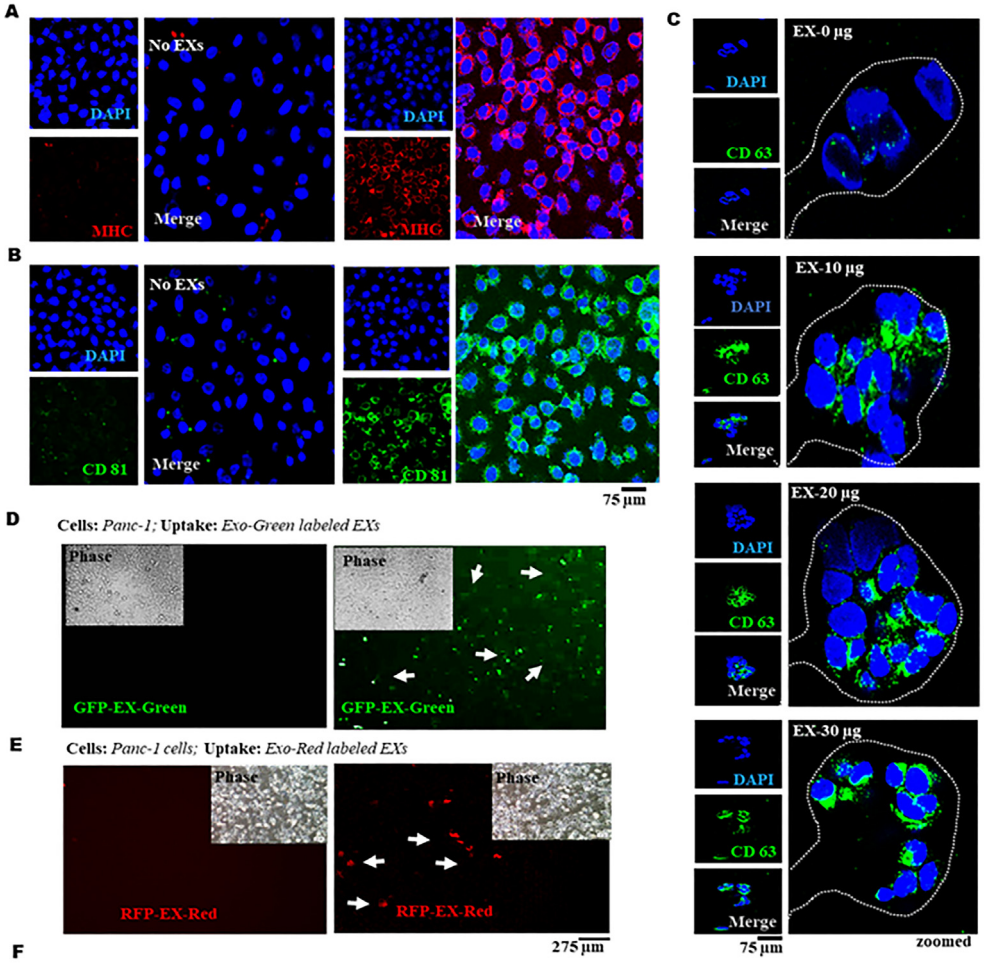

Inset table 1: ORM Loading efficacy of EXs from NAF/CAF

Cells	Protein	Drug Loading efficiency (%)	Drug content (µg/mL)
NAF	100 µg	21.23	212.346
	400 µg	84.06	841.282
CAF	100 µg	12.15	121.513
	400 µg	76.43	764.346

Inset table 2: Zeta potential and size of drug loaded EXs from NAF

Parameters		Formulation	Numbers
CAF-EX	Size	Empty	70.28 ± 1.47
		EX + ORM	215.6 ± 1.6
	Zeta	Empty	-25.35 mV
		EX + ORM	-17.3 mV
NAF-EX	Size	Empty	44.12 ± 0.89
		EX + ORM	272.25 ± 1.05
	Zeta	Empty	-14.9 mV
		EX+ ORM	-20.4 mV

Figure 2 Internalization of EXs in PanCa cells. Uptake of NAF-EX in cancer cells demonstrated by immunofluorescence assay. Exosomal protein marker (A) MHC (red) and (B) CD81 (green) expression representing uptake of EXs in cells. Scale bars are representative of 400 × magnification. DAPI stained nucleus is represented as blue (C) Uptake of NAF-EX (0, 10, 20, 30 µg) by HPAF-II cells determined by immunofluorescence. Exosomal marker CD63 expression (green color) has been used to identify exosomes in cells. Scale bars are representative of 400 × magnification. (D) NAF-EX uptake in PanCa cells determined by protein (GFP fluorescence) and (E) RNA (RFP fluorescence) respectively. Scale bars are representative of 100 × magnification. (F) Graphs representing %NAF and CAF drug loading efficiency at different concentrations of NAF-EX. Data represents mean ± SEM, $n = 5$; $^*P < 0.005$. (Inset table 1) Loading efficacy of EXs from NAF/CAF and (Inset table 2) Size and zeta potential of NAF-EX and NAF-EX-ORM particles, $n = 3$.

identify and select the best features that could help in finding discriminating set of proteins in CAF and NAF. The features have been selected using the method of Recursive feature elimination (RFE) class along with the Linear regression model to identify the correlation between the EXs from NAF and CAF. The implementation was done in python due to its extensive ability to analyze large

data set of data with better performance. The method RFE uses the Informed Greedy best first search algorithm to find out the best performing feature. Therefore, python selected and ranked the features from 1 to 403, 1 being the greater and 403 the lower to allow biologically relevant conclusions through differential expression analysis (Supporting Information Fig. S5). Overall analysis of our study selected 10 most significant and critical proteins (features) in CAF and NAF EXs that were ranked highest as 1 (Supporting Information Fig. S6 and Inset tables 1 and 2). This data is significant as these proteins can be further investigated for their clinical relevance in PDAC.

3.2. *NAF-EXs effectively target and internalize to PanCa cells*

Considering severe immune responses towards synthetic delivery system in human body, investigations on alternative delivery vehicle are highly desirable. In recent years EXs have shown great promise in this area especially, autologous EXs can be highly useful for minimizing immune responses and developing a personalized medicine approach to meet the individual patient's requirements. Thus, we also sought to investigate the ability of NAF-EXs to target and internalize into PanCa cells (HPAF-II and AsPC-1). Our data suggested that NAF-EXs (NAF-EX) effectively targets and efficiently internalized into the PanCa cells as determined by MHC (Fig. 2A) and CD81 (Fig. 2B) exosome marker expression as determined by confocal microscopy analysis. The cellular uptake was increased in concentrations (10, 20 and 30 μg of exosome protein) dependent manner in HPAF-II cells as determined by CD63 expression (Fig. 2C and Supporting Information Figs. S7A and S7B) in cells. NAF-EXs showed efficient cellular uptake and were internalized efficiently in sacks of cell organelles within the HPAF-II cells. To further confirm the cellular internalization of NAF-EXs, we loaded them with either 10x EX-Green (for proteins; GFP) or 10 × EX-Red (for RNAs; RFP). During each labeling reaction, a control reaction was performed using PBS not containing exosomes. Interestingly, both GFP and RFP cargo loaded NAFs EXs demonstrated very high internalization in PanCa cells within 24 h. The presence of green (carboxyfluorescein succinimidyl diacetate ester) and red (Acridine orange) fluorescence inside the cells revealed successful delivery of protein (Fig. 2D) and RNAs (Fig. 2E) cargoes in the cells by the NAF-EXs. Additionally, PDAC cells, HPAF-II was exposed to conditioned media (CM) obtained from CAFs and NAFs and accessed for internalization of the cell cargoes, particularly, miR-145. MiR-145-fold increase was observed in cells exposed to NAF-CM, max at 48 h (Supporting Information Fig. S8). These results suggest that NAF EVs internalize into the cancer cells as well as transfer their cargoes making distinct impact on cancer cells. The data also signifies that NAFs and CAFs vary in their characteristics/cargo and EXs released therefrom carry different molecules.

3.3. *NAF-EXs successfully functionalized with ORM and efficiently render its anti-cancer activity*

To determine drug functionalization capabilities of NAFs-EXs, we established a drug loading method using ORM as a model drug. We selected ORM for this formulation as it is safe for human use and we have recently shown its potent anti-cancer efficacy in PanCa model[10]. Several studies have showcased that exosome proteins within the range of 100−400 μg/mL are optimal for therapeutic delivery and biological significance[21−25]. In our studies, we also achieved highest drug loading efficiency with 400 μg exosome protein, therefore, we selected this concentration for our experiments. Our results suggest successful loading of ORM to NAFs-EXs. We achieved highest drug loading efficiency at 400 μg (84.06%) EXs protein concentration while lowest with 100 μg (21.23%). Whereas the drug loading efficiency of CAFs was comparatively much lower than NAF (Fig. 2F and Inset-table 1). The size and zeta potential of ORM functionalized NAF-EXs were determined by DLS. At maximum drug loading efficiency, NAFs-EXs demonstrated ∼272 nm size along with a zeta potential of −20.4 mV (Fig. 2F and Inset-table 2). Our results also demonstrated that the drug loading was higher with NAF-EXs as compared to CAF-EXs along with size variation (NAF-EXs-ORM 272.25 nm and CAF-EXs-ORM as 215.6 nm. However, there was no appreciable difference in the zeta potential of these formulations. Interestingly, size of the ORM loaded EXs was correlated with the drug loading efficiency. Our results also demonstrated that NAF-EXs have a relatively higher drug loading efficiency as compared to CAFs EXs. This further indicates the relevance of NAFs EXs for their utilization in delivering therapeutic cargoes.

Following performing necessary characterization assays, we evaluated *in vitro* therapeutic efficacy of the NAF-EXs-ORM formulation (NAF-EX-ORM) using PanCa cells (HPAF-II and AsPC-1). NAF-EX-ORM formulation effectively inhibited cellular growth of PanCa cells in a dose dependent manner, while unloaded formulation (NAF-EX) did not show any effect. Interestingly, NAF-EX-ORM formulation exhibited greater inhibition as compared to free ORM (Fig. 3A). These results were further confirmed by the real time xCELLigence system, which measures the electrical impedance by monitoring cell behavior such as cell number and morphology in a real time manner. Our results demonstrated potent growth inhibitory effects of NAF-EXs-ORM formulation in both AsPC1 (Fig. 3Bi) and HPAF-II (Supporting Information Fig. S9) cells. Additionally, we sought to investigate the effect of NAF-EXs-ORM formulation on invasive behavior of cells using xCELLigence assays (Fig. 3Bii). The xCELLigence Real-Time assay demonstrated inhibition in cellular invasion in AsPC-1 cells upon treatment with NAF-EX-ORM, which was confirmed by Matrigel invasion assay (Fig. 3Ci). Similar inhibitory effects were observed in migratory ability of cells due to NAF-EX-ORM treatment, which was observed using Boyden chamber assay (Fig. 3Cii). It was observed that NAF-EX-ORM formulation significantly decreased both the invasiveness and migration of pancreatic cancer cells compared to the control, EXs and free ORM at 48 h (Fig. 3Cii and Supporting Information Fig. S10A). These results were confirmed using tumorsphere assay, which showed that the formation of secondary tumorspheres was restricted following NAF-EX-ORM or ORM alone treatment in AsPC-1 and HPAF-II cells (Fig. 3D). Our results demonstrated that NAF-EX-ORM significantly reduced primary (Fig. 3Di and Fig. S10B) and secondary (Fig. 3Dii and Fig. S10C) tumor sphere size in both AsPC1 and HPAF-II cells. At the same time, a similar effect was observed in HPAF-II cells. These observations clinically validated our results by indicating the potential of NAF-EX-ORM to diminish spheroid formation which mimics a tumor model.

Moreover, we examined the effect of our formulation on cell cycle event and apoptotic index. Cell cycle analysis revealed remarkable alterations in different phases of cell cycle in response to the ORM and NAF-EX-ORM treatment in HPAF-II and AsPC-1 cells. NAF-EX-ORM formulation and ORM arrest cells in sub-G0 phase as suggested by sharp increase in number of cells in

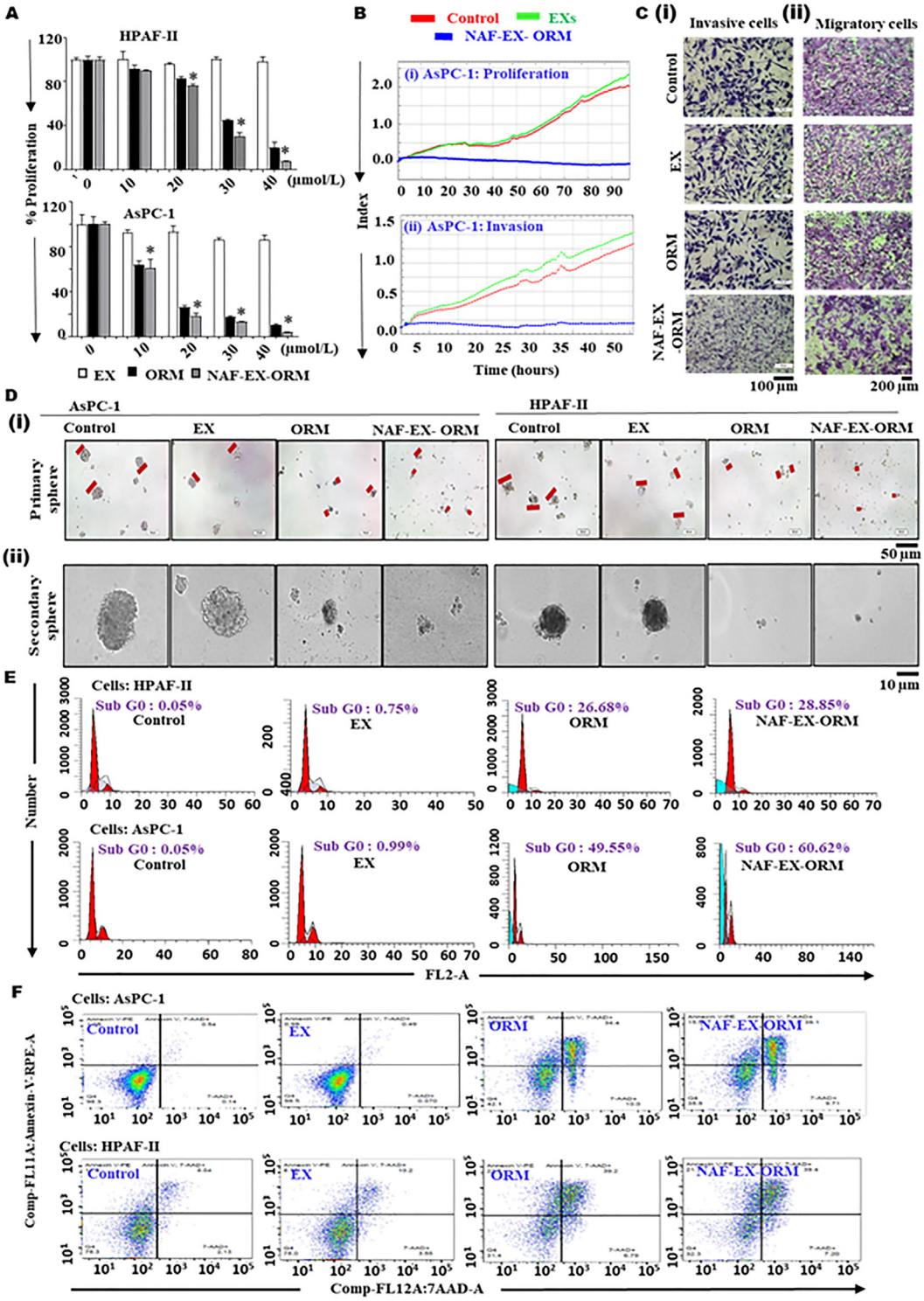

Figure 3 NAF-EXs loaded with ORM efficiently inhibit PanCa growth and invasion. (A) HPAF-II and AsPC-1 were treated with NAF-EXs, ORM (20 μmol/L) and NAF-EX-ORM (ORM: 20 μmol/L) in different concentrations. Graphs representing percent proliferation ability of both the cell lines following treatment as determined by MTT assay. Bars represent mean ± SEM, $n = 3$; $^*P < 0.05$. (B) Real time xCELLigence RTCA system demonstrating effect of treatment on PanCa cell proliferation and invasion. (C) Effect of treatment on metastatic characteristics of cells such as invasion using matrigel invasion assay and (i) migration using Boyden chamber assay (ii). (D) Effect of treatment on the formation of spheroid and their growth. HPAF-II and AsPC-1 were treated with EXs, ORM (20 μmol/L) and NAF-EX-ORM (ORM:20 μmol/L) in 96 well low attachment plate for 7 days to form (i) primary sphere and followed by 10 days to form. Scale bars are representative of 100 × magnification. (ii) Secondary sphere microscopy images show the size differences of tumor spheroids. Scale bars are representative of 200 × magnification. (E) PanCa cells treated with EXs, ORM and NAF-EX-ORM for 24 h show increased apoptotic population (Sub G0) and modulation of cell cycle phases and (F) demonstrate significant increase of early and total apoptotic population.

this phase, while an appreciable decline in S-phase (Fig. 3E). The data is quantified and shown in Supporting Information Fig. S11. We also observed an increased number of cells in early apoptotic phase, which suggests activation of apoptotic pathways by our formulation (Fig. 3F) in both HPAF-II and AsPC-1 cells. The quantified data is shown in Supporting Information Fig. S12. These results indicate that our formulation maintains the integrity of ORM, thus able to render its anti-cancer potential.

3.4. *NAF-EX-ORM formulation suppresses oncogenic signaling associated with pancreatic tumor environment*

Due to excessive desmoplasia (fibrosis) and poor vasculature, proper accumulation of therapeutic cargoes at tumor bed has been very challenging in pancreatic cancer. As a result of suboptimal drug accumulation, tumor acquire resistance to the therapies. Therefore, we sought to investigate the effect of ORM and NAF-EX-ORM on the desmoplastic markers on human pancreatic tumor derived stromal cells (CAFs). We observed that ORM and NAF-EX-ORM effectively repressed the expression of α-SMA, Desmin and hyaluronic acid as shown in our confocal microscopy analysis (Fig. 4A). Normal fibroblasts are typically tumor-suppressive but can be transformed into tumor-promoting cancer-associated fibroblasts (CAFs) through a series of phenotypic changes[26]. We investigated if ORM can prevent the transformation of normal fibroblasts into cancer fibroblasts. We utilized TGFβ1, which is characterized well as an inducer of cancer associated phenotype in normal fibroblasts. We observed that ORM inhibits TGFβ1 induced CAF activation, which was monitored by investigating some key proteins, such as fibroblast activation protein (FAP), fibronectin, tenascin-C and α-smooth muscle actin (α-SMA) (Fig. 4B). A concentration-dependent increase in all CAF markers was observed upon exposure to TGFβ1 treatment, which was significantly inhibited upon treatment with ORM. Therefore, our results suggested that ORM treatment can help in maintaining normal fibroblast cell phenotype and render them incompatible to be triggered for a CAF-like phenotype by TME signaling molecules, TGFβ1. This demonstrates the significance of ORM in inhibition of transformation of normal to cancerous phenotype. Additionally, we investigated the effect of NAF-EX-ORM on important oncogenic signaling pathway, which plays a key role in mediating stroma and cancer crosstalk entailing multiple downstream effectors that result in regulation of connecting pathways. Our immunoblot analyses suggest that ORM and NAF-EX-ORM formulations altered the expression of several proteins that are associated with desmoplasia (SHH, Gli and HAS 1), tumorigenesis/invasion (NFκB-p65, C-Myc), apoptosis (Bax, Bcl-2) and EMT (E-cadherin, N-cadherin, MMP2) (Figs. 4C and 5A). Relatively greater repression in the markers was observed upon NAF-EX-ORM treatment as compared with ORM alone, therefore, indicating a pronounced effect on stromal cells by ORM when shielded by exosome. Consistent with our published findings[10], our results indicate that NAF-EX-ORM effectively blocks the SHH signaling pathway by inhibiting the important effectors of this pathway, such as SHH, Gli-1, and NFκB-p65 in AsPC1 (Fig. 4C) and HPAF-II (Fig. 4D) cells and disrupts multiple paracrine factors, thus inhibits stromal and tumor cell crosstalk within the tumor. All these results confirmed that NAF-EX-ORM formulation can effectively repress desmoplasia and pancreatic tumor microenvironment.

Further investigations confirmed apoptosis as a mode of cell death, which included inhibition in Bcl-2 expression and activation of pro-apoptotic Bax expression in cells upon treatment with NAF-EX-ORM and ORM alone (Fig. 4C). The Bax expression was observed as increased and Bcl-2 expression as decreased with treatment of NAF-EX-ORM in both HPAF-II and AsPC-1 cells. Similar results were observed at mRNA level using PCR (Fig. 4D), where the Bcl2 mRNA levels were reduced whereas Bax levels increased upon treatment.

3.5. *NAF-EX-ORM inhibits propensity of PDAC cells to undergo EMT in response to EGF*

Epithelial−mesenchymal transition (EMT) has shown significant contribution in cancer metastasis and drug resistance[27]. The expression of EMT-inducing transcription factors is controlled by growth factor cytokine, which include Wnt, epidermal growth factor (EGF), Notch/delta and NF-κB pathways[28]. The EGF-induced EMT process is characterized by an increased expression of EMT-regulatory transcription factors, such as ZEB-1, SNAIL-1, SLUG, MMP proteins, N-cadherin and a decrease in epithelial cell surface marker, E-cadherin. In this study, we observed that NAF-EX-ORM switches the signaling molecules involved in Epithelial to Mesenchymal transition, such as upregulation of E-cadherin followed by the downregulation of N-cadherin and matrix metalloprotease-2 (MMP2), as observed through immunoblotting (Fig. 4C). Further investigation on changes in EMT related gene expression demonstrated the reduction in mRNA levels of N-cadherin, vimentin and c-myc (Fig. 5A) in both AsPC-1 and HPAF-II cells. Since this process is regulated by a complex network of signaling pathways and transcription factors, we sought to investigate if NAF-EX-ORM could influence EMT in PDAC. Therefore, we utilized recombinant EGF protein to stimulate EMT in PDAC cells as EGF is known to trigger EMT in pancreatic cancer cells and promote invasion and metastasis in cancer cells[29]. To determine the response of EGF on PanCa cells, we optimized the optimal concentration of EGF using its varying concentration of recombinant EGF (0−100 nmol/L) (Fig. 5B)[29]. It was observed that 100 nmol/L EGF showed maximum enhanced expression of important EMT markers (vimentin and N-cadherin) (Fig. 5B). Further, treatment of AsPC-1 cells with selected EGF concentration (100 nmol/L), demonstrated that EGF treatment effectively enhances cell proliferation as compared to control by 25% using MTT assay. Interestingly, the increase in proliferation due to EGF treatment was inhibited by treatment with ORM (75%) and NAF-EX-ORM (77%) (Fig. 5C). Additionally, ORM and NAF-EXs-ORM effectively blocked EGF induced cell migration, and invasion (Fig. 5 Di, ii), along with the expression of EMT markers (ZEB-1, SNAIL-1, SLUG, TWIST, vimentin, MMP-2, and vimentin) in a qPCR analysis (Fig. 5E and F). Altogether, these results suggest that NAF-EX-ORM treatment effectively downregulates PDAC progression by targeting EMT and SHH pathway *via* modulation of key downstream molecules of these pathways.

Keeping in view the significant function of ORM in modulating EMT processes during progression of cancer and preventing the transformation of normal to cancer fibroblasts (Fig. 4B), we sought to understand a mutual mechanism elicited by ORM that drives both the complexity and dynamics of events leading to metastasis. One of the important pathways in cellular phenotypic transitions is calcium (Ca^{2+}) signaling, which is known to be involved in the transformation of normal to cancerous fibroblasts[26]. One transformation that is Ca^{2+}signaling dependent is EMT[30]. Free intracellular Ca^{2+}acts as a second messenger to

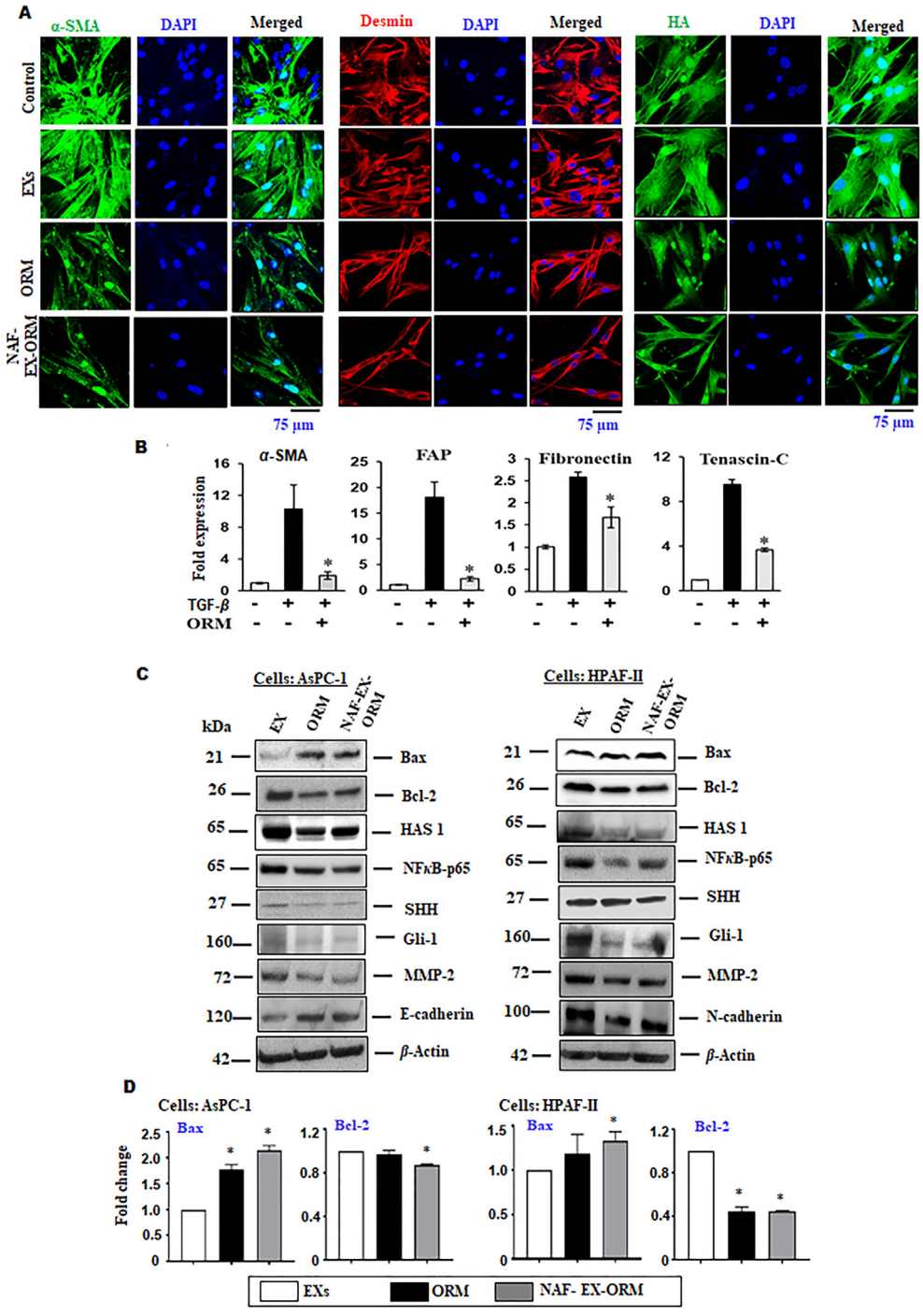

Figure 4 Suppression of reactive stroma microenvironment and inhibition in transformation of normal fibroblasts to cancerous phenotype. (A) CAF cells treated with ORM (20 μmol/L) and NAF-EX-ORM (ORM: 20 μmol/L) showed decreased expression of α-SMA, Desmin and hyaluronic acid (HA) in CAFs using confocal Immunofluorescence assay. Scale bars are representative of 400 × magnification. (B) TGFβ1 induced transformation of normal to cancerous phenotype in fibroblasts was abrogated by ORM (20 μmol/L) treatment as demonstrated by the restoring levels of αSMA, fibroblast activation protein (FAP), fibronectin, and tenascin-C upon treatment. Bars represent mean ± SEM, $n = 3$; $^*P < 0.05$. (C) Immunoblotting of EMT markers, SHH signaling pathway proteins and apoptotic proteins expression upon treatment with NAF-EXs-ORM (ORM: 20 μmol/L) and ORM (20 μmol/L) on AsPC-1 and HPAF-II cells. (D) qRT-PCR results demonstrate the Bax/Bcl2 expression in both HPAF-II and AsPC-1 cells upon treatment. Relative quantification of blots was represented by graph. Bars represent mean ± SEM, $n = 3$; $^*P < 0.05$.

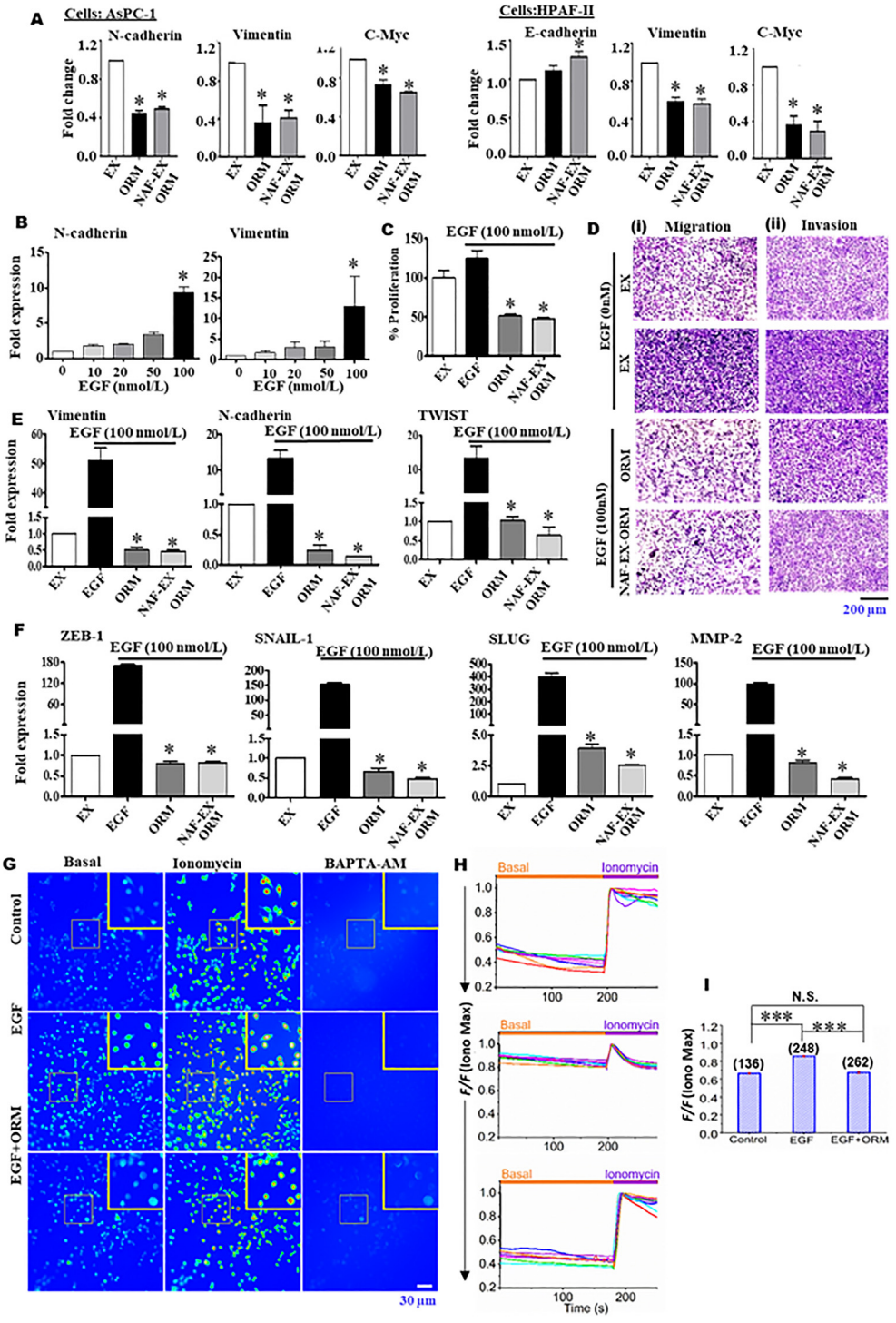

Figure 5 NAF-EX-ORM inhibits EMT and Ca^{2+} signaling. (A) Relative fold change in mRNA of key EMT pathway molecules by qRT-PCR upon treatment with EXs, ORM (20 µmol/L) and NAF-EX-ORM (ORM: 20 µmol/L). Bars represent mean ± SEM, $n = 3$; $^*P < 0.05$. (B) Optimization for EGF concentration using different concentrations of EGF (1−100 nmol/L). Bars represent mean ± SEM, $n = 3$; $^*P < 0.05$. (C) MTT assay in PanCa cells stimulated with EGF upon treatment with EXs, ORM (20 µmol/L) and NAF-EX-ORM (ORM: 20 µmol/L). Bars represent mean ± SEM, $n = 3$; $^*P < 0.05$. (D) Migration assay (i) and Invasion assay (ii) in presence of EGF (100 nmol/L) upon treatment with EXs, ORM (20 µmol/L) and NAF-EX-ORM (ORM: 20 µmol/L). Scale bars are representative of 200 × magnification. (E, F) mRNA expression of key proteins involved in EMT using qRT-PCR upon treatment with EXs, ORM (20 µmol/L) and NAF-EX-ORM (ORM: 20 µmol/L). Data represents mean ± SEM, $n = 3$; $^*P < 0.005$. (G−I) Fluorescence microscope image of cells treated with EGF alone or in presence of ORM (20 µmol/L) loaded with Fluo-4 AM before (basal; left) and after ionomycin (center) and BAPTA (right) application in cells (G). Representative Ca^{2+} imaging trace of cells showing basal Ca^{2+} fluorescence intensity (H). Ionomycin, a Ca^{2+} ionophore used to elicit a maximal Ca^{2+} signal, normalized to 1. (I) Graph analysis showing the basal Ca^{2+} level normalized to the ionomycin-induced maximum Ca^{2+} signal of data shown in H.

promote the growth and progression of cancer cells. As EGF is the predominant Ca^{2+} influx inducer in non-excitable cells, it activates downstream events leading to phospholipase C/inositol trisphosphate (IP3)/Ca^{2+} release from IP3-sensitive Ca^{2+} stores to modulate cell proliferation, motility, and invasion. We sought to investigate if ORM induced inhibition of normal to cancerous fibroblast phenotype involves remodeling of Ca^{2+}. Therefore, we performed live cell Ca^{2+} imaging in PDAC cells in presence of EGF stimulation to observe the effect of ORM treatment in cells. Measurement of Ca^{2+} levels in cell populations loaded with fluorescent indicator fluo-4/AM demonstrated that EGF elicited the increase of fluorescence intensity, which reflected the increase of Ca^{2+} at a dose of 10 ng/mL (Fig. 5Gi) as depicted by the images and the scatter plots using quantitative analysis (Fig. 5J–L). We observed that EGF induced transient Ca^{2+} increase in AsPC1 cells was inhibited in presence of ORM treatment in the cells. ORM restored the Ca^{2+} signal to the basal levels and demonstrated decreased relative Ca^{2+} signal as observed with EGF treatment. These observations open a new paradigm in a tumor progression model suggesting that stroma modulators may also regulate Ca^{2+} influx in fibroblast cells and thereby prevent the transformation of fibroblasts from normal to cancerous phenotype. Cancer fibroblasts are mediators of immunosuppression and inhibiting of CAFs *via* inhibition of TGF-β that enables infiltration of T cells to tumors/metastatic lesions, improving the response to immune checkpoint therapy and reducing tumor growth/metastasis[31]. Altogether, these studies indicate that CAFs perform a significant function in inhibiting tumor cell killing by T cells. This study further supports the importance of stroma inhibitors in the treatment of PDAC, which may regulate the tumor microenvironment and facilitate the efficient internalization of drug.

3.6. *Patient derived NAF EXs efficiently target pancreatic tumors*

Pancreatic tumor targeting has been very challenging, thus we sought to investigate if NAF-EXs can aid pancreatic tumor targeting. Investigators are trying several methods to improve the delivery of therapeutic agents to achieve the desired amounts to the tumor area such as pH Sensitive Drug Delivery Systems and antibody targeted monotherapies[32]. Although, significant progress has been made in the controlled drug delivery area, issues related to body's hyper immune reactivity, cytokine storming and upscaling of the complex delivery formulation methods have somewhat limited their scope in clinical practice. It would be highly beneficial if the active agents are delivered by a natural delivery system that can sense the impulse caused by disease, assessed the scale of signal, and deliver the payload at tumor bed site without causing hyper immune responses in the human body. Considering the genetic heterogeneity, diverse clonal origins, and higher mutational burden of tumors, such a system would require coupling of the drug delivery rate with the physiological need by the individual tumor. All these issues can be addressed by using autologous molecules using a personalized approach of medicine. In this respect, our results demonstrate that NAF-EXs can efficiently target pancreatic tumors. We tracked tumor targeting potential of NAF-EX through the conjugation of Indocyanine green dye (ICG dye) (NAF-EX-ICG) by *in vivo* molecular imaging (Fig. 6A). Our results show that ICG coupled NAF-EX (NAF-EX-ICG) specifically targeted pancreatic tumors, while the ICG alone was distributed into the whole body. The tumor targeting was visible as early as 6 h, being optimal at 48 h (Fig. 6A). These results are very promising as they open new avenues for an approach that can be translated into personalized medicine.

3.7. *NAF derived NAF-EX-ORM formulation repressed PDAC tumor in xenograft mouse model*

After growth assessment of efficient tumor targeting potential of NAF-EX-ICG, we evaluated therapeutic potential of our NAF-EX-ORM formulation using a PDAC xenograft mice model. For this experiment, human HPAF-II luciferase (HPAF-II-Luc) cells were subcutaneously injected in right flank of the mice. After 7 days of tumor cells injection, mice were randomly divided into three groups ($n = 6$). Mice were injected intraperitoneally with control (PBS), EX and NAF-EX-ORM (equivalent to 200 μg) (Fig. 6B). During experiment, male mice within the groups began to engage in fighting and cannibalism, even chewing tumors, thus those animals were removed from the group. As a result, the number was subsequently reduced in some groups. Despite the number discrepancy, we performed appropriate statistical analysis of collected data which is presented in the manuscript. In this study, NAF-EX-ORM treatment has shown severe reduction in tumor growth compared to control and EXs treated groups, as determined by bioluminescence imaging of whole-body mice (Fig. 6C), excised tumor (Fig. 6D) and other organs (Fig. 6E). This was reflected in physical detailed analysis of excised tumors (Fig. 6F). Analysis of *ex vivo* excised organs of mice demonstrated that NAF-EX-ORM treatment group showed no metastasis, whereas control treated groups showed metastasis in kidney, lungs, spleen (Fig. 6E). Mice treated with NAF-EX-ORM had significant reduction in tumor volume (Fig. 6G) and tumor weight (Fig. 6H) ($P < 0.05$) and improved survival. The impact of NAF-EVs was similar to the control group, and there was no noteworthy effect on inhibiting tumor growth. This is because NAF-EVs do not contain an optimal concentration of tumor suppressors capable of independently inducing tumor suppression in mice. The mice treated with NAF-EX-ORM exhibited exceptional overall survival, with no recorded deaths until the conclusion of the experiment. These mice were sacrificed upon reaching the experimental endpoint. Conversely, in the control and EX-treated groups, some mice had succumbed to the conditions before the experiment's conclusion (Supporting Information Fig. S13A).

Additionally, we conducted experiments to evaluate the biosafety of NAF-EVs-ORM. We assessed various parameters including animal behavior, body weight changes and histopathological examination of major organs. Our observations indicated no significant histopathological abnormalities or signs of toxicity in these organs (Fig. S13B). Additionally, our results indicate no changes in behavior or body weight in any of the treatment groups. Upon further investigation, we evaluated the protein

The different color lines in the graphs (H) represent the Ca^{2+} signals from multiple individual cells in each measurement; (N) denotes number of cells. Scale bar: 30 μm. The student's *t*-test was used for statistical analysis. The triple asterisk (***) indicates that differences between treatment and control groups are statistically significant (***$P < 0.0001$; n.s.: non-significant).

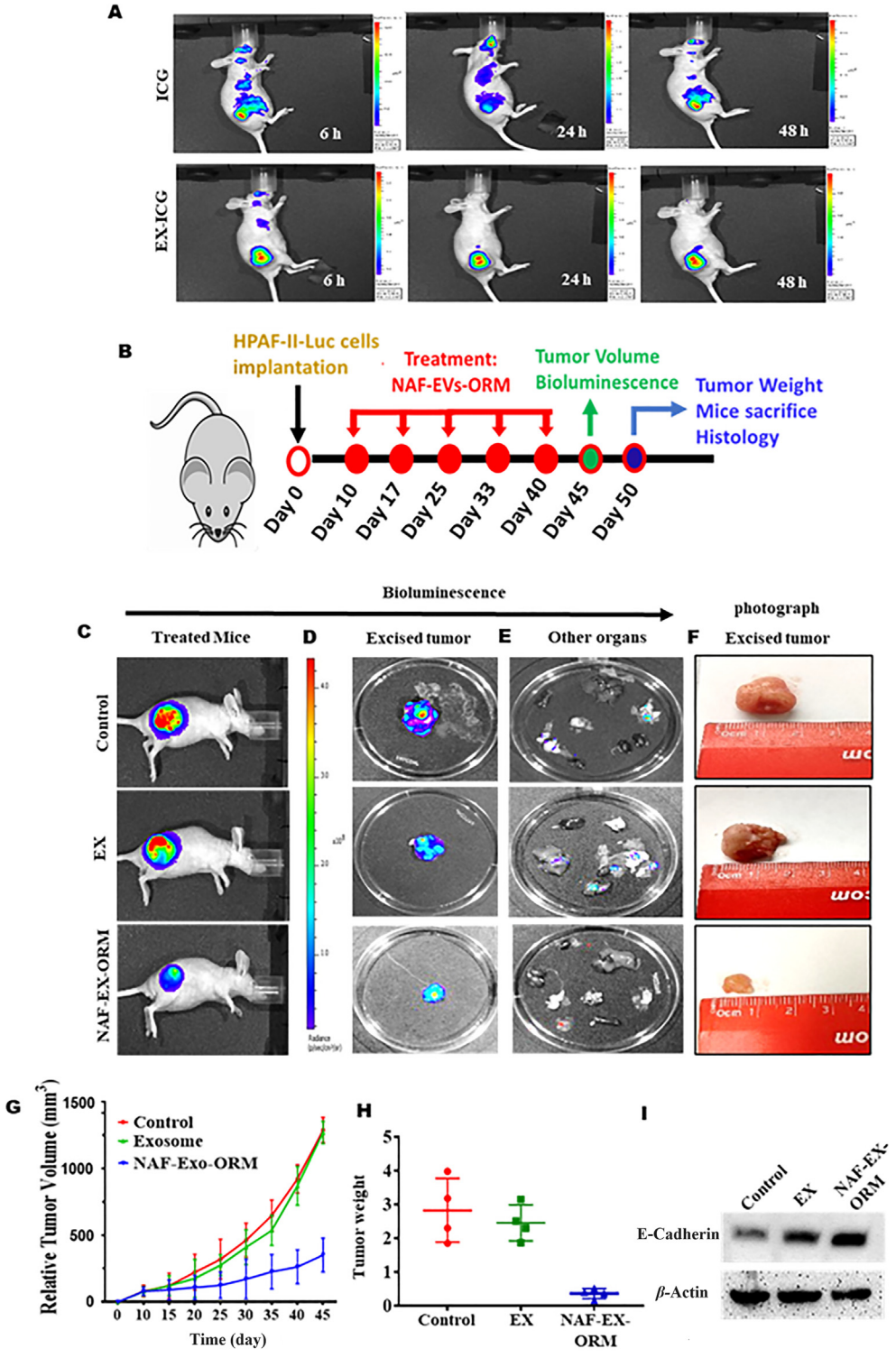

Figure 6 NAF-EXs target pancreatic tumor specifically in a mouse model and loaded ORM augments its therapeutic efficacy. (A) Demonstration of pancreatic tumor specific targeting of ICG using NAF-EXs by injecting EXs loaded with ICG or ICG alone intraperitonially in mice and photographed at different time points. (B) Schematic representation of tumor cell implantation and course of treatment performed in mice ($n = 6$). (C) Representative bioluminescence images of whole mice treated *via* i.p. with PBS as control (Group 1), free ORM (20 μmol/L) (Group 2) and NAF-EX-ORM (Group 3) (equivalent to 200 μg) (D) excised tumor images and (E) other organs. (F) Photograph image of the excised pancreatic tumor from mice. (G) Average tumor volume using vernier caliper and (H) tumor weight was observed. (I) Western blotting analysis indicating the effect of NAF EXs and NAF-EX-ORM on E-cadherin in excised tumors from all groups of mice.

expression of E-cadherin in an excised mice tumor of all treated groups. We found that NAF-EX-ORM treated group has increased expression of E-cadherin (Fig. 6H).

Confocal immunofluorescence and Immunohistochemistry analysis of the Formalin fixed paraffin embedded (FFPE) excised tissue sections showed reduced expression of α-SMA and hyaluronic acid, respectively, in mice treated with NAF-EX-ORM (Fig. 7A and E). We also observed inhibition in collagen-1 and vimentin expression and restoration of E-cadherin levels through immunofluorescence (Fig. 7B−D) in mice treated with NAF-EX-

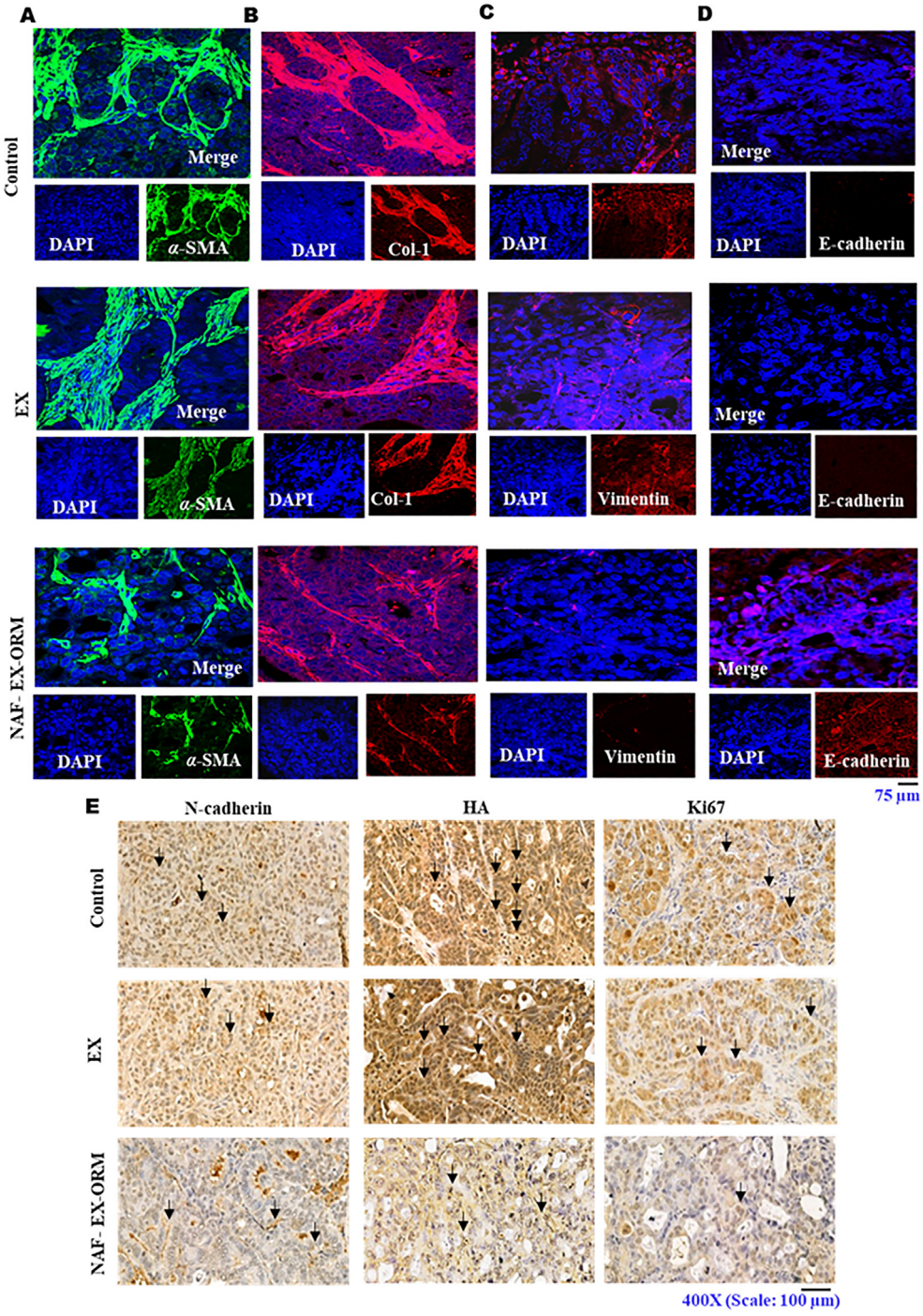

Figure 7 Immunofluorescent and immunohistochemical analysis of EMT and desmoplasia related protein markers in pancreatic tumor tissues from treated xenograft mice. Immunofluorescence staining and confocal microscopy images displayed the effect of EXs and NAF-EX-ORM treatment as compared to PBS treatment (control). NAF-EX-ORM inhibits stromal marker protein expression such as (A) αSMA and (B) collagen, (C) reduced expression of vimentin and (D) increased expression of E-cadherin. Images were captured at 400 $\times$. DAPI was used as a counter stain for the nucleus. (E) Immunohistochemical staining showing the inhibited expression of N-cadherin, hyaluronic acid (HA) and Ki67 in mice tumor tissue with NAF-EX-ORM treatment as compared to control and EXs (NAF-EX). Scale bars are representative of 200 $\times$ magnification.

ORM. Our results also suggested a decreased levels of N-cadherin and Ki67, β-catenin levels in tumor tissues of mice treated with NAF-EX-ORM as observed through immunohistochemistry (Fig. 7E and Supporting Information Fig. S14). Ki67 is known as a marker of proliferation and growth, which can also predict prognosis after treatment[33]. All these findings suggest that NAF-EXs delivered the ORM efficiently to the tumor and regulate key oncogenic processes in PDAC tumors.

4. Discussion

Newer treatment modalities for effective treatment and management are highly required to improve the treatment outcome of PDAC patients. Especially, management of the PDAC patient post-surgical resection requires more attention to increase the survival in the patients with localized tumors. Poor treatment outcome of PDAC patients is primarily attributed to the suboptimal accumulation of therapeutic payload at tumor bed that ultimately resulted to chemoresistance, tumor recurrence, and metastasis. Significant efforts are being made to improve the accumulation of payload in solid tumors using controlled drug delivery systems. However, hyper immune reactivity, cytokine storming and upscaling of the complex delivery formulation methods are some key issues associated with these synthetic systems. Thus, there is an urgent need to develop methods that can address these critical issues. In this study, we investigated the feasibility of a novel autologous biological delivery system that can improve tumor targeting, accumulation of therapeutic payload with no or minimal immune reactivity. As a biological delivery system, we used EXs that are isolated from the pancreatic tumor adjacent normal appearing fibroblasts (NAF-EXs). Our results suggest that NAF-EXs can efficiently target pancreatic tumors, deliver therapeutic payloads (ORM), and repress tumor growth *via* modulation of key oncogenic mechanisms of tumor microenvironment (TME). Our study opens a new avenue that can be explored for a personalized medicine approach using autologous EXs.

This study demonstrates the utilization of autologous exosomes derived from fibroblast cells isolated from NAF. This exosome based therapeutic intervention is especially suitable for the treatment of patients that are candidates for surgical removal of tumor. In this unique personalized medicine approach, patient derived NAF EXs will be used as biological vehicles for the delivery of a therapeutic agent(s) into the fibrotic PDAC tumor microenvironment, thereby remodeling the signals erupting thereof and preventing the formation of pre-metastatic niche. This strategy is highly required in reference to PDAC tumors that are characterized by excessive desmoplastic tumor microenvironment, low uptake of therapeutic payload, thus recurrence remains a big challenge. Therefore, we sought to investigate the utilization of NAF EXs as a unique scaffold for the delivery of a potent anticancer agent and stroma modulator, ORM, that we have recently identified in our lab[10]. In addition to tumor depleting properties, ORM inhibits TGFβ1 induced cancerous phenotype in normal fibroblast cells through remodeling of Ca^{2+} influx. The safety efficacy of this drug in humans has been thoroughly investigated and is a non-steroidal, non-hormonal anti-estrogen oral contraceptive safe for use in humans. Therefore, our study gives proof of concept and feasibility of utilization of this biological scaffold for effective therapeutics in combination with standard therapeutic regimen.

The utilization of EXs obtained from the NAF is based on the fact that the normal tissues surrounding the tumor area are in the most defensive and alert state in the body preventing them from neighboring malignant transformation. At this state, the normal tumor area would bear a responsive activation of molecular changes to fight against the sensed cellular and molecular factors driving transformation changes. This includes the inflammatory and metabolic changes that can suppress cancer in its initial state before the oncogenic conversion overtakes through the inter-issue/intercellular communications facilitated by extracellular vesicles and/or exosomes. Thus, the EXs derived from this area are biologically imprinted for tumor cell targeting and tumor suppression. Studies have reported the distinct biological characteristics and genetic heterogeneity among fibroblasts obtained from cancer (CAFs) and adjacent normal appearing area (NAFs)[34,35]. This was also observed in our experiments when exposing PDAC cells to conditioned media (CM) obtained from CAFs and NAFs, showed distinct impact on cancer cells. miR-145 expression was observed in HPAF-II (miR-145 absent cells) cells that were cultured in NAF CM compared with CAF CM (Fig. S7). On further investigation of CM, we found that the EXs from NAF CM has higher miR-145 expression in contrast to EXS from CAF CM (Fig. S2B). The data signifies that NAFs and CAFs vary in their characteristics/cargo and EXs released therefrom carry different molecules (Fig. S2A). Based on this observation, we performed proteomic analysis of EXs obtained from CAFs and NAFs. Our mass spectroscopy studies show that the EXs isolated from NAF have distinct cargo compared to CAF EXs, including increased expression of tumor suppressor miRNAs and decreased expression of some oncogenic miRNAs, which probably explain why NAF co-culture did not enhance tumorigenic features of PDAC cells. In fact, EXs isolated from NAFs demonstrated inhibitory effects on the EMT process, as evidenced by the repression of EMT markers. Therefore, this further contests the utilization of patient's autologous EXs for effective and targeted delivery of therapeutics.

Compared with the synthetic carriers such as nanoparticles, EXs as drug delivery systems exhibit several advantages like favorable biocompatibility, drug loading efficiency, tissue targeting ability, and the capability to cross biological barriers with very low or/no adverse immunogenic responses. In our drug loading experiments, we observed higher drug loading ability in NAF derived EXs at any concentration (100−400 μg) as compared to CAF derived EXs. Our NAF-EX-ORM formulation demonstrated higher cellular internalization in recipient PDAC cells, and effectively delivered therapeutic payload (ORM) to PDAC cells and tumors, as reflected by reduced tumorigenic features (such as proliferation, invasion and migration, increased apoptosis) (Fig. 2), tumor growth in xenograft mouse model (Fig. 6) and tumor desmoplasia markers (hyaluronan synthase, collagen-1, α-SMA and Desmin) (Fig. 7). Our previously published studies also reported inhibitory effects of ORM on SHH CXCL12/CXCR4 signaling pathways[10].

In addition to desmoplasia, EMT is another critical process required for tumor progression and metastasis, which is driven by numerous factors including activation of EGF/EGFR and Ca^{2+} signaling pathways[36]. This study for the first time demonstrates that NAF-EXO-ORM and ORM could block EGF-induced activation of EMT, associated proteins (vimentin, N-cadherin, Snail, Slug, MMP-2, Zeb-1 and Twist), Ca^{2+} ion uptake and inhibited EGF-stimulated metastatic features (invasion and migration) in PDAC cells. Altogether, our results highlight the unique capability of self-derived exosomes to act as a biological natural delivery

vehicle for drugs and ORM can effectively block desmoplastic and EMT processes in PDAC tumors. Thus, ORM can be a useful combination strategy to improve therapeutic efficacy of conventional and modern treatment modalities by improving their accumulation at the tumor bed. Our previous study has demonstrated that a combination of ORM and Gemcitabine provided an improved treatment outcome in PDAC cell line and mouse models[10]. The current findings further affirm the function of ORM and utilization of autologous exosomes for its effective presentation to diseased pancreas.

Selective pancreatic tumor targeting is an unmet clinical challenge. A recently published study showed favorable tumor targeting using plasma derived autologous EXs in CRC mouse model[37]. Considering this information, we sought to determine selective tumor targeting potential of NAFs derived EXs. Interestingly, our ICG conjugated NAF-EXs displayed highly selective and efficient tumor targeting in xenograft mouse model (Fig. 6). Previous studies in the field have demonstrated that EVs can employ both active and passive targeting mechanisms[38−40]. Active targeting refers to the specific recognition and binding of EVs to target cells through surface molecules or ligands that interact with receptors expressed on the target cells. Passive targeting, on the other hand, relies on the enhanced permeability and retention (EPR) effect, which allows EVs to accumulate at the tumor site due to the leaky vasculature and impaired lymphatic drainage commonly found in solid tumors[41,42]. Our data suggests preferential tropism of NAF derived EXs for PDAC tumors tissues, which suggests a targeted delivery approach. Altogether, data demonstrated in this manuscript implies feasibility of developing a novel personalized medicine for PDAC patients using autologous NAFs EXs for improved therapeutic outcome. Due to their natural origin and potential to facilitate intercellular communication in both local and distant microenvironments, autologous EXs might offer valuable insights for post-operative personalized medicine. Because of the targeted action, this approach will specifically deliver therapeutic payloads to the tumor site or diseased organ, while sparing normal, healthy organs/tissues in contrast to conventional therapies. They could serve as advanced platforms for potential applications in targeted drug/gene delivery. However, further studies are warranted in large preclinical models that are closer to humans to proceed with clinical translation of this unique approach.

5. Conclusions

In this study, we present a novel strategy to address the issues associated with conventional nanomedicine approach for PDAC tumor targeting and inaccessibility of drugs to fibrotic tumor site. Our research offers proof of the effectiveness of utilizing extracellular vesicles derived from cancer-associated fibroblasts (CAFs) for precise tumor targeting and drug delivery. It also points to the feasibility of their utilization in personalized medicine, reducing hyperimmune responses. Our study has successfully demonstrated the specific delivery of ORM, a potent anti-cancer and desmoplasia-inhibiting agent, to tumor sites.

Acknowledgments

The authors gratefully acknowledge Prof. Fathi Halaweish from University of South Dakota for synthesizing ormeloxifene drug. We also acknowledge Core facilities at UT-System. Authors acknowledge the following funding support from various agencies and foundation: UTRGV School of medicine start up, CPRIT TREC Award RP230419 and Integrated Cancer Research Core (ICRC)-RP210180; Herb Kosten foundation for pancreatic cancer research; National Institutes of Health grants R01CA206069, SC1GM139727, SC2GM139715, R01CA210192 and R01CA204552.

Author contributions

Sheema Khan, Subhash C. Chauhan, Stephen. W. Behrman: Conceptualization, Saini Setua, Shabia Shabir, Anupam Dhasmana, Junming Yu, Meena Jaggi, Sheema Khan, Subhash C. Chauhan, Stephen. W. Behrman, Nirakar Sahoo, Tripti Saini, Francesco Giorgianni, Andrew E Massey, Poornima Shaji, Ana Martinez Bulnes: Methodology, Saini Setua, Sheema Khan, Shabia Shabir, Subhash C. Chauhan, Swathi Holla, Poornima Shaji, Ana Martinez Bulnes, Anupam Dhasmana, Nivesh K. Mittal, Tripti Saini, Francesco Giorgianni, Meena Jaggi, Andrew E Massey, Vincent Diego, Bilal Hafeez, Manish Tripathi, Murali Mohan Yallapu: Investigation, Sheema Khan, Subhash C. Chauhan, Stephen. W. Behrman, Saini Setua, Shabia Shabir, Anupam Dhasmana: Visualization, Sheema Khan, Subhash C. Chauhan: Funding acquisition, Sheema Khan, Subhash C. Chauhan: Project administration, Sheema Khan, Subhash C. Chauhan, Stephen. W. Behrman: Supervision, Sheema Khan, Saini Setua: Writing − original draft, Sheema Khan, Subhash C. Chauhan, Stephen. W. Behrman, Shabia Shabir, Saini Setua, Murali Mohan Yallapu: Writing − review & editing.

Conflicts of interest

The authors declare that they have no known competing financial interests or personal relationships that could have appeared to influence the work reported in this paper.

Appendix A. Supporting information

Supporting information to this article can be found online at https://doi.org/10.1016/j.apsb.2024.04.003.

References

1. Lee JC, Ahn S, Cho IK, Lee J, Kim J, Hwang JH. Management of recurrent pancreatic cancer after surgical resection: a protocol for systematic review, evidence mapping and meta-analysis. *BMJ Open* 2018;**8**:e017249-57.
2. Sakamoto H, Attiyeh MA, Gerold JM, Makohon-Moore AP, Hayashi A, Hong J, et al. The evolutionary origins of recurrent pancreatic cancer. *Cancer Discov* 2020;**10**:792−805.
3. Ha D, Yang N, Nadithe V. Exosomes as therapeutic drug carriers and delivery vehicles across biological membranes: current perspectives and future challenges. *Acta Pharm Sin B* 2016;**6**:287−96.
4. Contreras-Naranjo JC, Wu HJ, Ugaz VM. Microfluidics for exosome isolation and analysis: enabling liquid biopsy for personalized medicine. *Lab Chip* 2017;**17**:3558−77.
5. An T, Qin S, Xu Y, Tang Y, Huang Y, Situ B, et al. Exosomes serve as tumour markers for personalized diagnostics owing to their important role in cancer metastasis. *J Extracell Vesicles* 2015;**4**:27522−36.
6. Pegtel DM, Cosmopoulos K, Thorley-Lawson DA, van Eijndhoven MA, Hopmans ES, Lindenberg JL, et al. Functional delivery of viral miRNAs *via* exosomes. *Proc Natl Acad Sci USA* 2010;**107**:6328−33.
7. Ran N, Li W, Zhang R, Lin C, Zhang J, Wei Z, et al. Autologous exosome facilitates load and target delivery of bioactive peptides to repair spinal cord injury. *Bioact Mater* 2023;**25**:766−82.

8. Yang C, Zhang M, Sung J, Wang L, Jung Y, Merlin D. Autologous exosome transfer: a new personalised treatment concept to prevent colitis in a murine model. *JCC* 2019;**14**:841−55.
9. Dai S, Wei D, Wu Z, Zhou X, Wei X, Huang H, et al. Phase I clinical trial of autologous ascites-derived exosomes combined with GM-CSF for colorectal cancer. *Mol Ther* 2008;**16**:782−90.
10. Khan S, Ebeling MC, Chauhan N, Thompson PA, Gara RK, Ganju A, et al. Ormeloxifene suppresses desmoplasia and enhances sensitivity of gemcitabine in pancreatic cancer. *Cancer Res* 2015;**75**:2292−304.
11. Bachem MG, Schneider E, Gross H, Weidenbach H, Schmid RM, Menke A, et al. Identification, culture, and characterization of pancreatic stellate cells in rats and humans. *Gastroenterology* 1998;**115**:421−32.
12. Dhasmana A, Uniyal S, Anukriti Kashyap VK, Somvanshi P, Gupta M, et al. Topological and system-level protein interaction network (PIN) analyses to deduce molecular mechanism of curcumin. *Sci Rep* 2020;**10**:12045−58.
13. Maher DM, Khan S, Nordquist JL, Ebeling MC, Bauer NA, Kopel L, et al. Ormeloxifene efficiently inhibits ovarian cancer growth. *Cancer Lett* 2015;**356**:606−12.
14. Sahoo N, Gu M, Zhang X, Raval N, Yang J, Bekier M, et al. Gastric acid secretion from parietal cells is mediated by a Ca^{2+} efflux channel in the tubulovesicle. *Dev Cell* 2017;**41**:262−73.
15. Khan S, Setua S, Kumari S, Dan N, Massey A, Hafeez BB, et al. Superparamagnetic iron oxide nanoparticles of curcumin enhance gemcitabine therapeutic response in pancreatic cancer. *Biomaterials* 2019;**208**:83−97.
16. Khan S, Zafar N, Khan SS, Setua S, Behrman SW, Stiles ZE, et al. Clinical significance of MUC13 in pancreatic ductal adenocarcinoma. *HPB (Oxford)* 2018;**20**:563−72.
17. Piffoux M, Nicolas-Boluda A, Mulens-Arias V, Richard S, Rahmi G, Gazeau F, et al. Extracellular vesicles for personalized medicine: the input of physically triggered production, loading and theranostic properties. *Adv Drug Deliv Rev* 2019;**138**:247−58.
18. Cancer Genome Atlas Research Network. The molecular taxonomy of primary prostate cancer. *Cell* 2015;**163**:1011−25.
19. Aran D, Camarda R, Odegaard J, Paik H, Oskotsky B, Krings G, et al. Comprehensive analysis of normal adjacent to tumor transcriptomes. *Nat Commun* 2017;**8**:1077−90.
20. Zhang J, Li S, Li L, Li M, Guo C, Yao J, et al. Exosome and exosomal microRNA: trafficking, sorting, and function. *Dev Reprod Biol* 2015;**13**:17−24.
21. Tian Y, Li S, Song J, Ji T, Zhu M, Anderson GJ, et al. A doxorubicin delivery platform using engineered natural membrane vesicle exosomes for targeted tumor therapy. *Biomaterials* 2014;**35**:2383−90.
22. Gomari H, Forouzandeh Moghadam M, Soleimani M. Targeted cancer therapy using engineered exosome as a natural drug delivery vehicle. *OncoTargets Ther* 2018;**11**:5753−62.
23. Bagheri E, Abnous K, Farzad SA, Taghdisi SM, Ramezani M, Alibolandi M. Targeted doxorubicin-loaded mesenchymal stem cells-derived exosomes as a versatile platform for fighting against colorectal cancer. *Life Sci* 2020;**261**:118369−78.
24. Hosseini NF, Amini R, Ramezani M, Saidijam M, Hashemi SM, Najafi R. AS1411 aptamer-functionalized exosomes in the targeted delivery of doxorubicin in fighting colorectal cancer. *Biomed Pharmacother* 2022;**155**:113690.
25. Qi J, Zhou Y, Jiao Z, Wang X, Zhao Y, Li Y, et al. Exosomes derived from human bone marrow mesenchymal stem cells promote tumor growth through hedgehog signaling pathway. *Cell Physiol Biochem* 2017;**42**:2242−54.
26. Sadras F, Stewart TA, Robitaille M, Peters AA, Croft PK, Soon PS, et al. Altered calcium influx pathways in cancer-associated fibroblasts. *Biomedicines* 2021;**9**:680−92.
27. Li L, Qi L, Liang Z, Song W, Liu Y, Wang Y, et al. Transforming growth factor-β1 induces EMT by the transactivation of epidermal growth factor signaling through HA/CD44 in lung and breast cancer cells. *Int J Mol Med* 2015;**36**:113−22.
28. Loh CY, Chai JY, Tang TF, Wong WF, Sethi G, Shanmugam MK, et al. The E-Cadherin and N-Cadherin switch in epithelial-to-mesenchymal transition: signaling, therapeutic implications, and challenges. *Cells* 2019;**8**:1118−50.
29. Buonato JM, Lan IS, Lazzara MJ. EGF augments TGF beta-induced epithelial−mesenchymal transition by promoting SHP2 binding to GAB1. *J Cell Sci* 2015;**128**:3898−909.
30. Davis FM, Azimi I, Faville RA, Peters AA, Jalink K, Putney JW, et al. Induction of epithelial−mesenchymal transition (EMT) in breast cancer cells is calcium signal dependent. *Oncogene* 2014;**33**:2307−16.
31. Monteran L, Erez N. The dark side of fibroblasts: cancer-associated fibroblasts as mediators of immunosuppression in the tumor microenvironment. *Front Immunol* 2019;**10**:1835−49.
32. Wen H, Jung H, Li X. Drug delivery approaches in addressing clinical pharmacology-related issues: opportunities and challenges. *AAPS J* 2015;**17**:1327−40.
33. Li LT, Jiang G, Chen Q, Zheng JN. Ki67 is a promising molecular target in the diagnosis of cancer (Review). *Mol Med Rep* 2015;**11**:1566−72.
34. Peng Q, Zhao L, Hou Y, Sun Y, Wang L, Luo H, et al. Biological characteristics and genetic heterogeneity between carcinoma-associated fibroblasts and their paired normal fibroblasts in human breast cancer. *PLoS One* 2013;**8**:e60321-33.
35. Santi A, Kugeratski FG, Zanivan S. Cancer associated fibroblasts: the architects of stroma remodeling. *Proteomics* 2018;**18**:1700167−81.
36. Sheng W, Chen C, Dong M, Wang G, Zhou J, Song H, et al. Calreticulin promotes EGF-induced EMT in pancreatic cancer cells *via* Integrin/EGFR-ERK/MAPK signaling pathway. *Cell Death Dis* 2017;**8**:e3147−60.
37. Villa A, Garofalo M, Crescenti D, Rizzi N, Brunialti E, Vingiani A, et al. Transplantation of autologous extracellular vesicles for cancer-specific targeting. *Theranostics* 2021;**11**:2034−47.
38. Shao J, Zaro J, Shen Y. Advances in exosome-based drug delivery and tumor targeting: from tissue distribution to intracellular fate. *Int J Nanomed* 2020;**15**:9355−71.
39. Choi H, Yim H, Park C, Ahn SH, Ahn Y, Lee A, et al. Targeted delivery of exosomes armed with anti-cancer therapeutics. *Membranes* 2022;**12**:85−101.
40. Wang Z, Mo H, He Z, Chen A, Cheng P. Extracellular vesicles as an emerging drug delivery system for cancer treatment: current strategies and recent advances. *Biomed Pharmacother* 2022;**153**:113480−94.
41. Yallapu MM, Jaggi M, Chauhan SC. Scope of nanotechnology in ovarian cancer therapeutics. *J Ovarian Res* 2010;**3**:19−28.
42. Golombek SK, May JN, Theek B, Appold L, Drude N, Kiessling F, et al. Tumor targeting *via* EPR: strategies to enhance patient responses. *Adv Drug Deliv Rev* 2018;**130**:17−38.